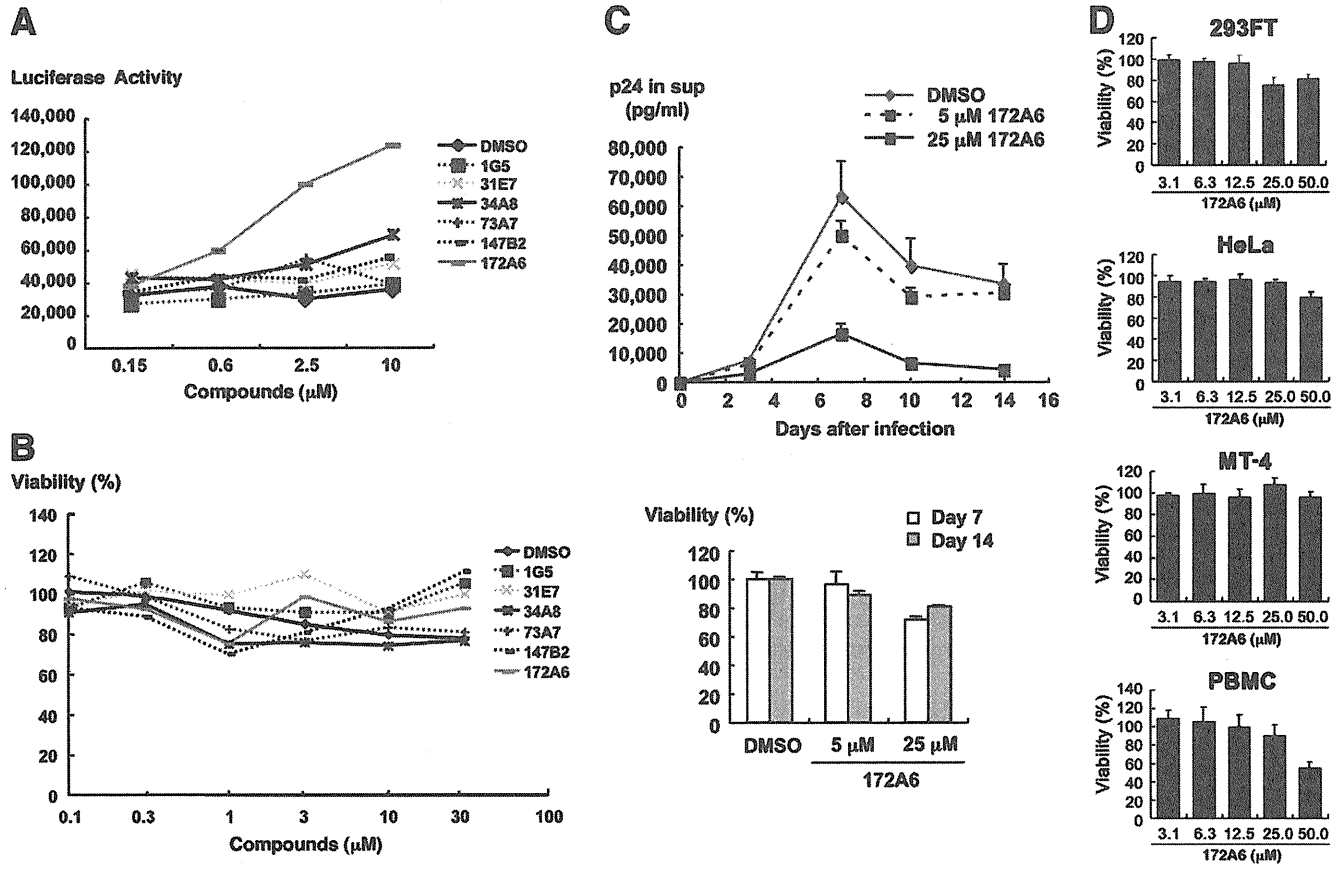

FIG. 3. Inhibition of HIV-1 replication and cell toxicity. (A) MT-4 Luc cells were infected with HIV-1 (HXB2 strain) and incubated at 37°C in the presence of increasing doses of compounds. On day 7, MT-4 Luc cells were subjected to luciferase assay. Data were shown as means from triplicate cultures. (B) 293T cells were incubated with various doses of compounds at 37°C for 2 days and subjected to Alamar Blue assays. Data were shown as means from 3 independent experiments. (C) PBMC stimulated with IL-2 and anti-CD3 antibody were infected with HIV-1 (HXB2 strain) and incubated at 37°C in the presence of 5 and 25 μM 172A6. HIV-1 production in culture medium was temporally quantified by p24CA antigen capture ELISA (top). Uninfected PBMC were cultured with 172A6 at 37°C and were subjected to MTS assay on days 7 and 14. Data were shown as means with standard deviations from triplicate cultures, in which DMSO was used as control. (D) 293FT, HeLa, and MT-4 cells and PBMC were incubated at 37°C with various doses of 172A6 and were subjected to MTS assay on days 4, 3, 4, and 6, respectively. Cell viability was shown as OD_{490}. Data were shown as means with standard deviations from triplicate cultures.

microscopy (Fig. 4B). HeLa cells were transfected with a pNL43 derivative that expresses Gag-GFP and incubated with 30 μM BMMP. Gag-GFP was distributed predominantly at the plasma membrane in cells treated with DMSO (used as control). A similar Gag-GFP distribution was observed in cells treated with BMMP, indicating that BMMP did not inhibit Gag targeting to the plasma membrane, consistent with the above findings.

Inhibition of HIV replication postentry by BMMP. To examine whether BMMP exerted an inhibitory effect on early stages of the HIV life cycle, such as viral entry, we employed single-round infection assays with luciferase-expressing HIV-1 vectors which were pseudotyped with either VSV-G or authentic HIV-1 Env protein. To this end, pHIVgag-pol (for expression of HIV-1 Gag and Gag-Pol), pRevpac (for expression of HIV-1 Rev), and pLenti-luciferase vector, which provides the artificial lentiviral genome expressing luciferase driven by cytomegalovirus promoter, were cotransfected with either VSV-G or authentic HIV-1 Env expression plasmid into 293FT cells. HIV-1 Luc viruses produced were inoculated into MT-4 cells in the presence of BMMP, and viral infectivity was monitored by a luciferase reporter assay. Luciferase expression was inhibited in a BMMP dose-dependent manner in cells infected with the HIV-1 Env-pseudotyped Luc virus, indicating that BMMP inhibited the early stage of the HIV-1 life cycle (Fig. 5A). However, when VSV-G-pseudotyped Luc virus was used, a dose-dependent reduction was similarly observed. When HIV-1 (NL43 strain) expressing luciferase was pseudotyped with VSV-G and used in this assay, the luciferase activity driven by the LTR promoter was similarly reduced in the presence of BMMP, suggesting that BMMP did not inhibit the stage of HIV entry (e.g., attachment and membrane fusion processes) but the stage of postentry (e.g., uncoating) (Fig. 5A). The Env-independent infectivity reduction was confirmed when HIV-1 Luc viruses were inoculated into 293FT and 293FT-CD4 cells (Fig. 5B). We examined whether BMMP also blocked the postentry stage of SIV. Interestingly, single-round infection assays with luciferase-expressing SIVmac239 vectors which were pseudotyped with VSV-G protein showed no inhibition of luciferase expres-

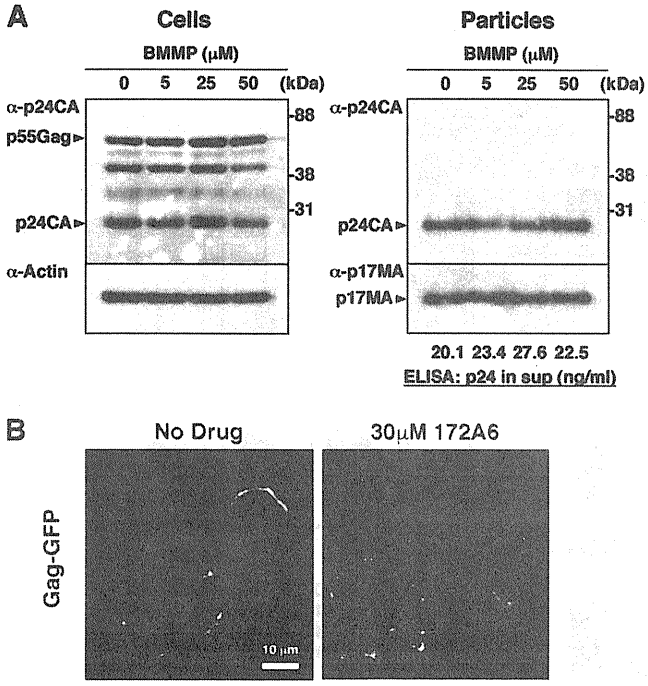

FIG. 4. HIV-1 particle production and Gag plasma membrane targeting. (A) Effects on HIV-1 particle production. 293FT cells were transfected with pHXB2 and incubated at 37°C with 0 to 50 μM BMMP. Two days posttransfection, cells were collected and culture media were subjected to purification of viral particles by ultracentrifugation. Equivalent volumes of samples were subjected to SDS-PAGE followed by Western blotting using anti-HIV-1 p24CA antibody. Representative blots were shown. HIV-1 particle yields in culture media were quantified by p24CA antigen capture ELISA. (B) Intracellular localization of Gag. HeLa cells were transfected with a pNL43 derivative in which Gag was fused with GFP and incubated at 37°C for 1.5 days with 30 μM BMMP. Nuclei were stained with TO-PRO-3, and cells were observed by confocal microscopy. Representative images were shown at the same magnification. Bar = 10 μm.

sion (Fig. 5B). No reduction in luciferase expression was also observed when luciferase-expressing pseudotyped MLV was used (data not shown). These data suggest that BMMP specifically inhibits HIV replication postentry but not those of other retroviruses, such as SIV and MLV.

To confirm the postentry block prior to particle production, we isolated cellular DNA from MT-4 cells infected with HIV-1 (HXB2 strain) that were treated with BMMP. Then, we quantified early reverse transcripts of HIV (corresponding to the strong-stop DNA), late reverse transcripts of HIV, and integrated HIV DNA by PCR. When normalized to the level of β-globin DNA (internal control), the levels of the early and late reverse transcripts and of the integrated proviral DNA were reduced, as observed for cells treated with 200 nM efavirenz controls (Fig. 5C). However, RT enzymatic activity was not affected by BMMP when examined in *in vitro* assays (data not shown). Together, these data indicate that BMMP blocks the early stage of the HIV-1 life cycle, preventing the completion of reverse transcription.

Mapping of Gag domain targeted by BMMP. To map the HIV Gag domain responsible for the postentry block by BMMP, a series of chimeric Gag constructs between HIV-1 and SIVmac239 were made in the context of pHIVgag-pol. HIV-1 MA, MACA, and CA were replaced by SIV MA, MACA, and CA, respectively (referred to as sMA, sMACA, and sCA, respectively). These Gag/Gag-Pol expression plasmids were cotransfected with pRevpac and pLenti-luciferase vector, and viruses were pseudotyped with VSV-G protein. Western blotting using anti-HIV-1 p17MA and p24CA and anti-SIVmac p27CA antibodies revealed that, although the anti-HIV-1 p24CA antibody that we used was cross-reactive with SIV CA, each domain of Gag was replaced in the chimeric constructs and virus particles were produced at levels largely similar to that of the wild type of HIV-1 Gag construct (Fig. 6A). Single-round infection assays with these Gag chimeras revealed that BMMP inhibited viral infection postentry only when HIV-1 CA was present in the constructs (Fig. 6B). Thus, our data indicated that BMMP inhibited the early stage of HIV-1 replication in a CA-specific and species-specific manner. These phenotypes resemble those observed for the CA-specific retroviral restriction imposed by a host factor, tripartite motif protein 5 (TRIM5) (30). HIV-1 CA is known to bind a host factor, CypA, likely through amino acids G89 and P90 in the exposed loop of CA (15, 16). This binding facilitates the early stage of HIV-1 replication prior to reverse transcription (9). Interestingly, HIV/SIV chimera studies have shown that the CypA-binding site overlaps with the determinants for species-specific restriction (30, 34). Thus, we made an HIV-1 Gag construct containing amino acid substitutions G89A and P90A in the CypA-binding loop of CA (referred to as CypA mt) and tested the sensitivity to BMMP. The CypA mt did not display the resistance to BMMP (Fig. 6B), suggesting that HIV-1 inhibition by BMMP was not linked to the CypA binding or TRIM5. No firm conclusions were drawn from mapping experiments using Gag chimeras within CA, i.e., N- and C-terminal domains (NTD and CTD), since the CTD mutant showed a lower yield of particle production (data not shown).

Disassembly of HIV capsid core by BMMP. The chimera experiments showed that the CA domain is critical for the inhibitory effect of BMMP on the early stage of HIV-1 replication. Thus, we examined whether BMMP affects CA-CA interaction using purified CA. An *in vitro* assembly reaction with purified HIV-1 CA was employed to test if BMMP disrupted CA-CA interactions. *In vitro* assembly reaction of CA has shown it to produce tubular structures representing the mature CA capsid structure (17, 36). We added BMMP to the *in vitro* assembly reaction with 100 μM HIV-1 CA, and resultant CA assembly products were observed by electron microscopy (Fig. 7A). For quantitative analysis, the resultant CA assembly products were recovered by ultracentrifugation and subjected to SDS-PAGE. The levels of the CA assembly products were reduced when BMMP was added at a concentration higher than 30 μM, corresponding to approximately a 1:3 molar ratio to CA (Fig. 7A). These data suggest that BMMP targets HIV-1 CA and leads to the destabilization of the viral capsid core, since our previous findings indicated that BMMP did not block particle release (Fig. 4) but did block the HIV-1 infection postentry (Fig. 5).

To test this possibility in a more relevant assay, we adopted cell-free disassembly assays using purified HIV-1 mature capsid core. To this end, we isolated HIV-1 capsid cores by ultracentrifugation through a Triton X-100 layer, as described pre-

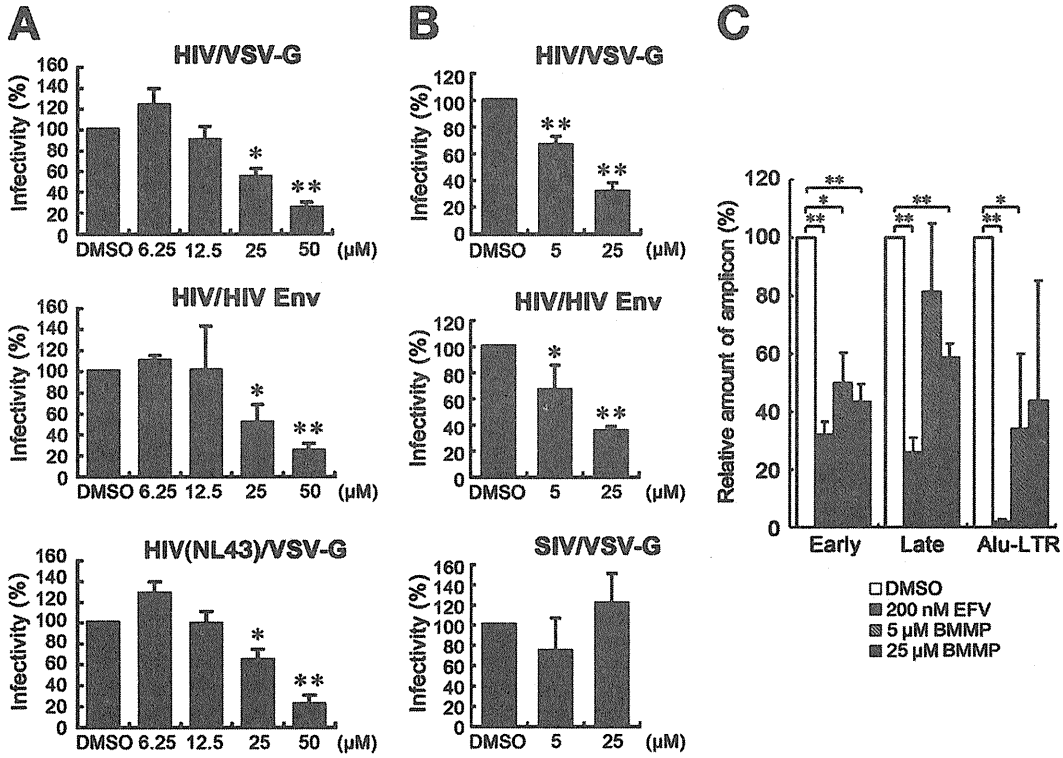

FIG. 5. Inhibition of HIV-1 replication postentry. (A) Single-round infection assays in MT-4 cells. 293FT cells were cotransfected with pHIVgag-pol (derived from HXB2 strain), pLenti-luciferase, pRevpac, and either a plasmid expressing HIV-1 Env (middle) or a plasmid expressing VSV-G (top). HIV-1 (NL43 strain) expressing luciferase was similarly pseudotyped with VSV-G protein (bottom). Following incubation, the culture supernatants were recovered and were subsequently inoculated into MT-4 cells with increasing doses of BMMP. (B) Single-round infection assays in 293FT and 293FT-CD4 cells. HIV-1 vectors containing the luciferase gene were similarly pseudotyped with HIV-1 Env (middle) or VSV-G protein (top). Luciferase-expressing SIVmac was pseudotyped with VSV-G protein by cotransfection (bottom). Viruses produced were subsequently inoculated into 293FT (top and bottom) or 293FT-CD4 (middle) cells with 5 and 25 μM BMMP. Viral infectivity was assessed by luciferase reporter assays. Data were shown as means with standard deviations from 3 to 6 independent experiments in panels A and B. *, $P < 0.05$; **, $P < 0.01$. (C) Quantitative PCR. MT-4 cells were infected with HIV-1 (HXB2 strain) and incubated in the presence of BMMP. DNA was isolated at 4 or 24 h postinfection and subjected to quantitative PCR for HIV cDNA. Reverse transcripts generated at the early and late phases of HIV reverse transcription were amplified from the DNA isolated at 4 and 24 h postinfection, respectively. The integrated viral genome was amplified as *Alu*-LTR transcripts from the DNA isolated at 24 h postinfection. EFV (200 nM) was used as positive controls. Three independent infections were performed, and quantitative PCR was carried out in triplicate with each infection sample. Representative data were shown with the means and standard deviations. *, $P < 0.05$; **, $P < 0.01$.

viously (3). HIV-1 cores are known to disassemble when incubated at 37°C. We examined if BMMP accelerated the rate of core disassembly. The HIV-1 cores were incubated with BMMP at 37°C up to 120 min, and residual intact cores were recovered by centrifugation. When quantified by p24CA antigen capture ELISA, intact cores were found to be reduced in a time-dependent manner in the presence of DMSO (as control), consistent with previous reports (3). A similar level of reduction was observed in the presence of AZT. However, addition of BMMP accelerated a reduction in intact cores in a dose-dependent manner (Fig. 7B). Altogether, our data indicated that BMMP disrupted HIV-1 capsid cores through targeting CA.

DISCUSSION

In this study, we employed a yeast membrane-associated two-hybrid assay to monitor the HIV Gag-Gag interactions and established cell-based screening assays for drugs targeting Gag assembly. We screened a commercially available chemical library and found BMMP, which inhibits HIV-1 replication in PBMC culture. Our single-round infection analysis indicated that BMMP primarily targets HIV-1 CA and inhibits HIV infection postentry but not particle production (Fig. 4 to 6). *In vitro* CA assembly/disassembly assays showed that BMMP facilitated HIV-1 core disassembly (Fig. 7). Collectively, it is conceivable that BMMP may bind to mature capsid structure and facilitate disassembly of the capsid, leading to premature earlier uncoating and failure of postentry events (e.g., reverse transcription and integration). The mechanism of action may be akin to the block of HIV-1 entry by rTRIM5α (30).

Previous studies have reported inhibitors that target HIV-1 Gag assembly and/or Gag processing. 3-*O*-(3′,3′-Dimethylsuccinyl)betulinic acid, known as PA-457 or Bevirimat (molecular weight, 584), binds to the Gag CA-SP1 cleavage site and inhibits proteolytic conversion of Gag precursors to the mature form of p24CA (50% inhibitory concentration [IC_{50}] = 10 nM) (1, 2, 21). Inhibition of Gag processing has also been observed with a distinct chemical class of compound, 1-[2-(4-tert-butylphenyl)-2-(2,3-dihydro-1H-inden-2-ylamino)ethyl]-3-(trifluoro-

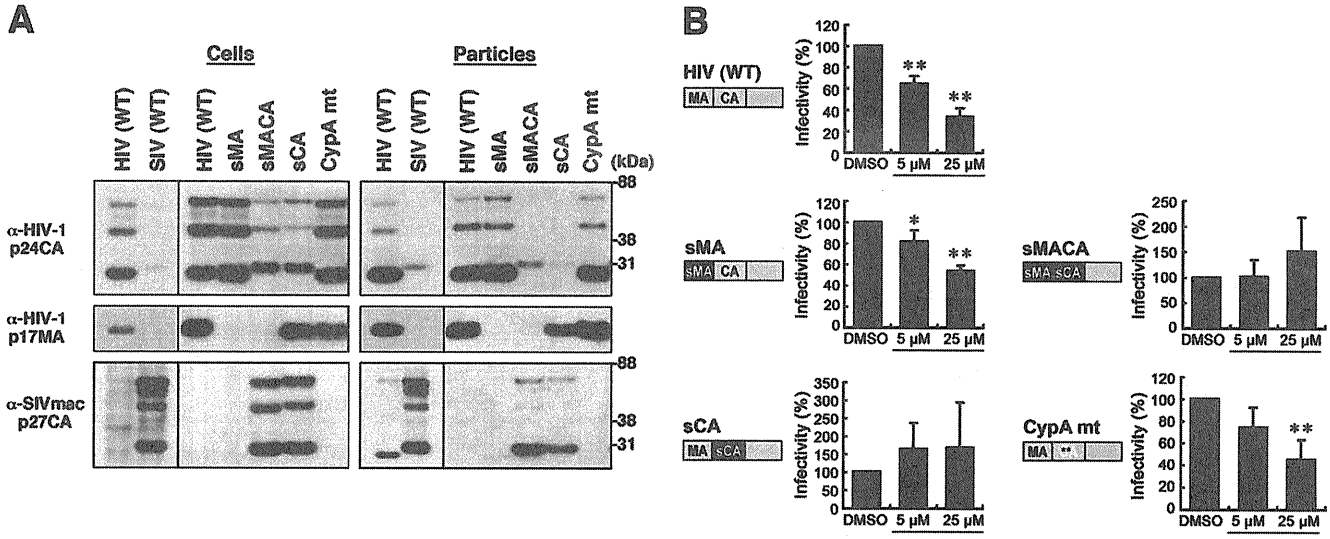

FIG. 6. Mapping of Gag domain responsible for inhibition. (A) Intracellular Gag expression and particle production. 293FT cells were cotransfected with pHIVgag-pol expressing chimeric Gag, pLenti-luciferase, pRevpac, and a plasmid expressing VSV-G, and virus particles produced were purified by ultracentrifugation. Cells and particles were analyzed by Western blotting using anti-HIV-1 p24CA and p17MA and anti-SIVmac p27CA antibodies. (B) Single-round infection assays with the Gag domain chimeras and Gag mutants with amino acid substitutions. The corresponding domain of SIVmac Gag (black) was introduced into HIV-1 Gag background (gray), and the resultant chimera was referred to as "s" plus the name of the corresponding domain of SIVmac. WT, wild type; sMA, HIV containing replacement of MA with SIV MA; sMACA, HIV containing replacement of MACA with SIV MACA; sCA, HIV containing replacement of CA with SIV CA. CypA mt represents HIV with amino acid substitutions G89A and P90A in the CypA-binding loop of CA NTD (denoted by asterisks). Following infection, the cell culture was incubated in the presence of 5 and 25 μM BMMP. Viral infectivity was monitored by luciferase reporter assays. Data were shown as means with standard deviations from 4 to 6 independent experiments. *, $P < 0.05$; **, $P < 0.01$.

methyl)pyridin-2(1H)-one (molecular weight, 454) (7). The hallmark of these inhibitors is incomplete Gag processing and accumulation of processing intermediates (e.g., CA-SP1) in virions, resulting in the loss of viral infectivity. These compounds do not inhibit Gag assembly. Since our BMMP did not show alteration in overall patterns of Gag processing (Fig. 4A), it is unlikely that BMMP shares the inhibition mechanisms with above inhibitors.

Inhibitors of HIV capsid assembly have been extensively screened by several approaches. *In silico* screening from public chemical libraries has identified *N*-(3-chloro-4-methylphenyl)-*N'*-{2-[({5-[(dimethylamino)-methyl]-2-furyl}-methyl)-sulfanyl] ethyl}-urea, termed CAP-1 (32), which binds to HIV-1 CA NTD (K_d [dissociation constant] = 800 μM), resulting in the inhibition of the correct interaction of hexameric units of CA NTD with dimeric units of CA CTD, essential for a high order of CA assembly (20). CAP-1 reduced the infectivity of progeny HIV but did not inhibit viral entry or particle production (32). Phage display biopanning has also been employed and has isolated a 12-mer peptide, termed CAI, which binds to HIV-1 CA CTD (50% inhibitory concentration [IC_{50}] = 3 to 4 μM) and inhibits CA capsid formation *in vitro* (K_d = 15 μM) (5, 29, 33). However, CAI did not inhibit HIV replication in cell culture because of the lack of cell permeability. In a subsequent study, CAI has been converted to a cell-penetrating peptide (termed NYAD-1) by stabilizing the α-helical structure of CAI with a hydrocarbon staple, leading to a marked improvement of K_d (<1 μM) (38). Surprisingly, the study revealed that, besides inhibiting the particle production, NYAD-1 disrupted the mature core formation and inhibited the early stage of HIV-1 in single-round infection assays, suggesting that NYAD-1 may affect the uncoating stage of the HIV life cycle through a mechanism similar to that of BMMP.

The difference between BMMP and CAI/NYAD-1 is that BMMP does not affect HIV-1 particle production or maturation steps. This is possibly because BMMP inhibits CA-CA interactions more efficiently than Gag-Gag interactions. Importantly, BMMP is not a peptide but a low-molecular-weight compound (molecular weight, 273.38), which is chemically and physically stable. It should be possible to chemically modify the BMMP structure to potentiate its biochemical and biological activities. The advantage of BMMP is that, due to its low molecular weight, the derivatives could retain cell membrane permeability unless large chemical groups are attached to the core structure.

A low-molecular-weight Gag inhibitor, PF74, previously screened from a chemical library by a high-throughput single-round infection assay (6), has been characterized by a more recent study, in which PF74 selectively inhibited HIV-1 (27). PF74 destabilized HIV-1 capsids and inhibited the postentry events, similarly to BMMP, but at low-micromolar concentrations. However, BMMP is distinct from PF74 in that the CypA-binding loop is not involved in the viral susceptibility to BMMP (Fig. 6B). Also, BMMP did not reduce the viral infectivity when the virion was exposed to BMMP (data not shown). Therefore, BMMP may have a potential to serve as a lead compound for the development of anti-HIV drugs bearing a novel mechanism of action.

Although BMMP showed anti-HIV activity, it still needs to be improved to lower the IC_{50}. We suggest that comprehensive studies on structural analogues of BMMP would be informative to understand the structure-function relationship of

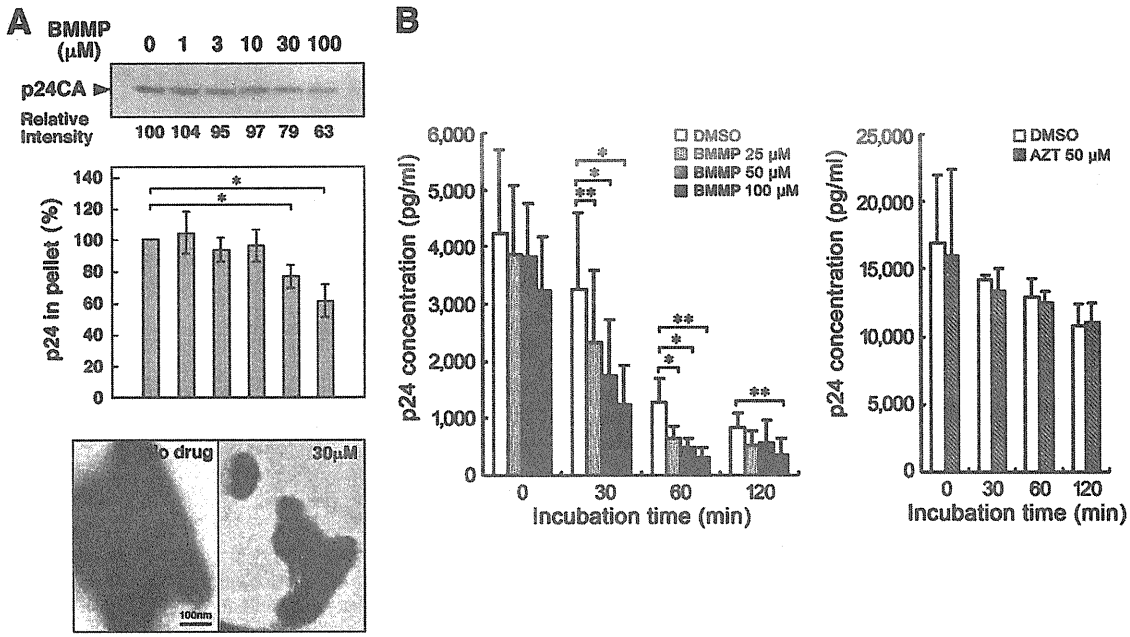

FIG. 7. HIV-1 mature capsid disassembly and *in vitro* assembly assays. (A) *In vitro* assembly reaction with purified HIV-1 CA. Purified HIV-1 CA protein (100 μM) was incubated with various doses of BMMP at 37°C for 60 min in buffer at high salt concentration. All samples included 1% DMSO. Assembly products were recovered by centrifugation and subjected to SDS-PAGE followed by Coomassie brilliant blue staining. The band intensities were semiquantified by ImageJ software. For quantification, the pelleted products were subjected to p24CA antigen capture ELISA. Data were shown as means with standard deviations from 3 independent experiments. *, $P < 0.05$. Assembly products were also negatively stained and examined by electron microscopy. Micrographs were shown at the same magnification. Bar = 100 nm. (B) Cell-free assays for HIV-1 uncoating. HIV-1 mature capsids were isolated through a 1% Triton X-100 layer as described previously (3). The HIV-1 cores were incubated with various doses of BMMP at 37°C up to 120 min. For comparison, the cores were similarly incubated with 50 μM AZT. All samples included 1% DMSO. Residual intact cores were recovered by ultracentrifugation and quantified by p24CA antigen capture ELISA. Data were shown as means with standard deviations from 4 independent experiments. *, $P < 0.05$; **, $P < 0.01$.

BMMP. Also, analysis of BMMP-resistant viruses and X-ray cocrystallography should provide insights into the mechanism of action that direct the way to potentiate the BMMP derivatives.

Recent cryo-electron microscopy and X-ray structure analysis have revealed the intermolecular interfaces between NTD and CTD in the three-dimensional hexameric structures of full-length CA (18, 24). It has been strongly suggested that multiple CA interactions, including NTD-NTD, CTD-CTD, and NTD-CTD, are essential for the constitution of mature HIV capsid. It is possible that some of the interfaces may not be formed in Gag-Gag interactions. CAI, similar to CAP-1, may inhibit CA assembly possibly by disrupting the formation of the NTD-CTD interface (18). Thus, these studies may provide a rationale for developing inhibitors that target the molecular interface of CA that specifically appears during a higher order of oligomerization. We suggest that viral capsid assembly/disassembly is an attractive therapeutic target and that such capsid inhibitors would help understand the regulation of postentry events.

ACKNOWLEDGMENTS

This work was supported by a Human Science grant from the Ministry of Health, Labor, and Welfare of Japan and by a Grant-in-Aid for Scientific Research from the Japan Society for the Promotion of Science.

REFERENCES

1. **Adamson, C. S., et al.** 2006. In vitro resistance to the human immunodeficiency virus type 1 maturation inhibitor PA-457 (Bevirimat). J. Virol. **80:** 10957–10971.
2. **Adamson, C. S., K. Waki, S. D. Ablan, K. Salzwedel, and E. O. Freed.** 2009. Impact of human immunodeficiency virus type 1 resistance to protease inhibitors on evolution of resistance to the maturation inhibitor bevirimat (PA-457). J. Virol. **83:**4884–4894.
3. **Aiken, C.** 2009. Cell-free assays for HIV-1 uncoating. Methods Mol. Biol. **485:**41–53.
4. **Aronheim, A., et al.** 1994. Membrane targeting of the nucleotide exchange factor Sos is sufficient for activating the Ras signaling pathway. Cell **78:**949–961.
5. **Bartonova, V., et al.** 2008. Residues in the HIV-1 capsid assembly inhibitor binding site are essential for maintaining the assembly-competent quaternary structure of the capsid protein. J. Biol. Chem. **283:**32024–32033.
6. **Blair, W. S., et al.** 2005. A novel HIV-1 antiviral high throughput screening approach for the discovery of HIV-1 inhibitors. Antiviral Res. **65:**107–116.
7. **Blair, W. S., et al.** 2009. New small-molecule inhibitor class targeting human immunodeficiency virus type 1 virion maturation. Antimicrob. Agents Chemother. **53:**5080–5087.
8. **Botstein, D.** 1997. Yeast as a model organism. Science **277:**1259–1260.
9. **Braaten, D., E. K. Franke, and J. Luban.** 1996. Cyclophilin A is required for an early step in the life cycle of human immunodeficiency virus type 1 before the initiation of reverse transcription. J. Virol. **70:**3551–3560.
10. **Broder, S.** 2010. The development of antiretroviral therapy and its impact on the HIV-1/AIDS pandemic. Antiviral Res. **85:**1–18.
11. **Bukovsky, A. A., A. Weimann, M. A. Accola, and H. G. Gottlinger.** 1997. Transfer of the HIV-1 cyclophilin-binding site to simian immunodeficiency virus from *Macaca mulatta* can confer both cyclosporin sensitivity and cyclosporin dependence. Proc. Natl. Acad. Sci. U. S. A. **94:**10943–10948.
12. **Butler, S. L., M. S. T. Hansen, and F. D. Bushman.** 2001. A quantitative assay for HIV DNA integration *in vivo*. Nat. Med. **7:**631–634.
13. **Craven, R. C., and L. J. Parent.** 1996. Dynamic interactions of the Gag polyprotein. Curr. Top. Microbiol. Immunol. **214:**65–94.
14. **Forshey, B. M., U. von Schwedler, W. I. Sundquist, and C. Aiken.** 2002.

Formation of a human immunodeficiency virus type 1 core of optimal stability is crucial for viral replication. J. Virol. **76:**5667–5677.
15. **Franke, E. K., H. E. Yuan, and J. Luban.** 1994. Specific incorporation of cyclophilin A into HIV-1 virions. Nature **372:**359–362.
16. **Gamble, T. R., et al.** 1996. Crystal structure of human cyclophilin A bound to the amino-terminal domain of HIV-1 capsid. Cell **87:**1285–1294.
17. **Ganser, B. K., S. Li, V. Y. Klishko, J. T. Finch, and W. I. Sundquist.** 1999. Assembly and analysis of conical models for the HIV-1 core. Science **283:** 80–83.
18. **Ganser-Pornillos, B. K., A. Cheng, and M. Yeager.** 2007. Structure of full-length HIV-1 CA: a model for the mature capsid lattice. Cell **131:**70–79.
19. **Graf Einsiedel, H., et al.** 2002. Deletion analysis of $p16^{INKa}$ and $p15^{INKb}$ in relapsed childhood acute lymphoblastic leukemia. Blood **99:**4629–4631.
20. **Kelly, B. N., et al.** 2007. Structure of the antiviral assembly inhibitor CAP-1 complex with the HIV-1 CA protein. J. Mol. Biol. **373:**355–366.
21. **Li, F., et al.** 2003. PA-457: a potent HIV inhibitor that disrupts core condensation by targeting a late step in Gag processing. Proc. Natl. Acad. Sci. U. S. A. **100:**13555–13560.
22. **Morikawa, Y.** 2003. HIV capsid assembly. Curr. HIV Res. **1:**1–14.
23. **Pauwels, R., et al.** 1990. Potent and selective inhibition of HIV-1 replication in vitro by a novel series of TIBO derivatives. Nature **343:**470–474.
24. **Pornillos, O., et al.** 2009. X-ray structures of the hexameric building block of the HIV capsid. Cell **137:**1282–1292.
25. **Roberts, N. A., et al.** 1990. Rational design of peptide-based HIV proteinase inhibitors. Science **248:**358–361.
26. **Sakuragi, S., T. Goto, K. Sano, and Y. Morikawa.** 2002. HIV type 1 Gag virus-like particle budding from spheroplasts of *Saccharomyces cerevisiae*. Proc. Natl. Acad. Sci. U. S. A. **99:**7956–7961.
27. **Shi, J., J. Zhou, V. B. Shah, C. Aiken, and K. Whitby.** 2011. Small molecule inhibition of human immunodeficiency virus type 1 infection by virus capsid destabilization. J. Virol. **85:**542–549.
28. **Shimizu, S., et al.** 2007. Inhibiting lentiviral replication by HEXIM1, a cellular negative regulator of the CDK9/cyclin T complex. AIDS **21:**575–582.
29. **Sticht, J., et al.** 2005. A peptide inhibitor of HIV-1 assembly *in vitro*. Nat. Struct. Mol. Biol. **12:**671–677.
30. **Stremlau, M., et al.** 2006. Specific recognition and accelerated uncoating of retroviral capsids by the TRIM5alpha restriction factor. Proc. Natl. Acad. Sci. U. S. A. **103:**5514–5519.
31. **Suzuki, S., et al.** 2010. Peptide HIV-1 integrase inhibitors from HIV-1 gene products. J. Med. Chem. **53:**5356–5360.
32. **Tang, C., et al.** 2003. Antiviral inhibition of the HIV-1 capsid protein. J. Mol. Biol. **327:**1013–1020.
33. **Ternois, F., J. Sticht, S. Duquerroy, H. G. Krausslich, and F. A. Rey.** 2005. The HIV-1 capsid protein C-terminal domain in complex with a virus assembly inhibitor. Nat. Struct. Mol. Biol. **12:**678–682.
34. **Towers, G. J., et al.** 2003. Cyclophilin A modulates the sensitivity of HIV-1 to host restriction factors. Nat. Med. **9:**1138–1143.
35. **Urano, E., et al.** 2008. Substitution of the myristoylation signal of human immunodeficiency virus type 1 Pr55Gag with the phospholipase C-delta1 pleckstrin homology domain results in infectious pseudovirion production. J. Gen. Virol. **89:**3144–3149.
36. **von Schwedler, U. K., et al.** 1998. Proteolytic refolding of the HIV-1 capsid protein amino-terminus facilitates viral core assembly. EMBO J. **17:**1555–1568.
37. **Westby, M., G. R. Nakayama, S. L. Butler, and W. S. Blair.** 2005. Cell-based and biochemical screening approaches for the discovery of novel HIV-1 inhibitors. Antiviral Res. **67:**121–140.
38. **Zhang, H., et al.** 2008. A cell-penetrating helical peptide as a potential HIV-1 inhibitor. J. Mol. Biol. **378:**565–580.

Biochemical and Biophysical Research Communications 404 (2011) 822–828

Contents lists available at ScienceDirect

Biochemical and Biophysical Research Communications

journal homepage: www.elsevier.com/locate/ybbrc

Distinct fucosylation of M cells and epithelial cells by Fut1 and Fut2, respectively, in response to intestinal environmental stress

Kazutaka Terahara [a], Tomonori Nochi [b], Masato Yoshida [b], Yuko Takahashi [b], Yoshiyuki Goto [b], Hirotsugu Hatai [b], Shiho Kurokawa [b], Myoung Ho Jang [c], Mi-Na Kweon [d], Steven E. Domino [e], Takachika Hiroi [f], Yoshikazu Yuki [b], Yasuko Tsunetsugu-Yokota [a], Kazuo Kobayashi [a], Hiroshi Kiyono [b,*]

[a] Department of Immunology, National Institute of Infectious Diseases, 1-23-1 Toyama, Shinjuku-ku, Tokyo 162-8640, Japan
[b] Division of Mucosal Immunology, Department of Microbiology and Immunology, The Institute of Medical Science, The University of Tokyo, 4-6-1 Shirokanedai, Minato-ku, Tokyo 108-8639, Japan
[c] Laboratory of Gastrointestinal Immunology, World Premier International Immunology Frontier Research Center, Osaka University, 3-1 Yamada-oka, Suita, Osaka 565-0871, Japan
[d] Mucosal Immunology Section, International Vaccine Institute, Seoul 151-818, Republic of Korea
[e] Department of Obstetrics and Gynecology, The University of Michigan Medical School, 6428 Medical Science Bldg I, 1150 West Medical Center Drive, Ann Arbor, MI 48109-5617, USA
[f] Department of Allergy and Immunology, The Tokyo Metropolitan Institute of Medical Science, 2-1-6 Kamikitazawa, Setagaya-ku, Tokyo 156-8506, Japan

ARTICLE INFO

Article history:
Received 13 December 2010
Available online 21 December 2010

Keywords:
Epithelial cell
Fucosyltransferase
Intestine
M cell
Peyer's patch

ABSTRACT

The intestinal epithelium contains columnar epithelial cells (ECs) and M cells, and fucosylation of the apical surface of ECs and M cells is involved in distinguishing the two populations and in their response to commensal flora and environmental stress. Here, we show that fucosylated ECs (F-ECs) were induced in the mouse small intestine by the pro-inflammatory agents dextran sodium sulfate and indomethacin, in addition to an enteropathogen derived cholera toxin. Although F-ECs showed specificity for the M cell-markers, lectin *Ulex europaeus* agglutinin-1 and our monoclonal antibody NKM 16-2-4, these cells also retained EC-phenotypes including an affinity for the EC-marker lectin wheat germ agglutinin. Interestingly, fucosylation of Peyer's patch M cells and F-ECs was distinctly regulated by α(1,2)fucosyltransferase Fut1 and Fut2, respectively. These results indicate that Fut2-mediated F-ECs share M cell-related fucosylated molecules but maintain distinctive EC characteristics, Fut1 is, therefore, a reliable marker for M cells.

1. Introduction

M cells are generally observed in the follicle-associated epithelium (FAE) of mucosa-associated lymphoid tissues including Peyer's patches (PPs) and isolated lymphoid follicles (ILFs) in the small intestine [1,2], and are morphologically and functionally distinct from their neighboring epithelial cells (ECs) by the presence of relatively short and irregular microvilli on their apical surface and of lymphocytes and antigen-presenting cells frequently enfolded within a pocket structure in their basolateral region [3–5]. In the small intestine of mice, the expression of α(1,2)fucose is believed to be a reliable marker of M cells, because lectin *Ulex europaeus* agglutinin-1 (UEA-1), which has an affinity for α(1,2)fucose, was found to bind exclusively to M cells in the PPs [6,7]. Subsequently, we could found M cells located within the non-FAE-associated small intestinal villous epithelium by utilizing an affinity of UEA-1 [8].

Interestingly, α(1,2)fucosylation is also induced in ileal villous ECs by a variety of intestinal environmental stresses (IES) such as colonization by commensal bacteria, weaning, mechanical injury or treatment with chemicals inhibiting protein synthesis [9–11]. When considering the possible involvement of IES in the development of (or conversion to) M cells, it is reasonable to postulate that such fucosylated ECs form a subset of M cells, because the number of PP M cells is increased rapidly and transiently by alteration from specific pathogen-free (SPF) conditions to a conventional environment [12], by interaction with bacteria such as *Salmonella typhimurium* [13] and *Streptococcus pneumoniae* [14] and during indomethacin-induced ileitis [15]. Like PP M cells, villous M cells might also be induced (or converted) by IES, because a higher frequency of villous M cells is observed in the terminal ileum, which is enriched for commensal bacteria [16]. Recently, we found that some ECs underwent α(1,2)fucosylation in the small intestinal villous epithelium when a mucosal adjuvant cholera toxin (CT) derived from a well known enteropathogen *Vibrio cholerae* was orally administered into mice, and that these cells, in part, shared the same gene expression profile as PP M cells; we previously designated them "M-like cells" [17].

In mice, α(1,2)fucosyltransferase Fut1 and Fut2 are the enzymes responsible for catalyzing an α(1,2) linkage of fucose to terminal β-galactoside, and Fut2 is involved in the IES-associated fucosylation

* Corresponding author. Fax: +81 3 5449 5411.
E-mail address: kiyono@ims.u-tokyo.ac.jp (H. Kiyono).

0006-291X/$ - see front matter © 2010 Elsevier Inc. All rights reserved.
doi:10.1016/j.bbrc.2010.12.067

whereas little is known about Fut1 in the intestine [11,18–20]. In this study, we aimed to elucidate the biological characteristics of ECs that shared the α(1,2)fucose modification with M cells focusing on the fucosylation mechanism, in the hope of better understanding of whether ECs can be reprogrammed into M (or M-like) cells in response to IES.

2. Materials and methods

2.1. Mice

BALB/c and C57BL/6J mice were purchased from SLC (Shizuoka, Japan). Fut1-null and Fut2-null mice (C57BL/6J background) were generated as previously described [21]. These mice were maintained under SPF conditions and used in experiments at 6–9 weeks old. All animal experiments were approved by the Animal Care and Use Committee of The University of Tokyo.

2.2. Lectins and antibodies

The following lectins and antibodies were used for flow cytometry (FCM) and confocal laser scanning microscopy (CLSM): PE-conjugated UEA-1 (UEA-1-PE; Biogenesis, England, UK), tetramethylrhodamine isothiocyanate (TRITC)-conjugated UEA-1 (Vector Laboratories, Burlingame, CA), Alexa Fluor 633-conjugated wheat germ agglutinin (WGA-AF633; Molecular Probes, Eugene, OR), FITC-conjugated NKM 16-2-4 mAb (NKM 16-2-4-FITC) [22], APC-conjugated anti-mouse CD45 mAb (anti-CD45-APC; BD Biosciences, San Jose, CA).

2.3. Alteration of the intestinal environment

A mucosal adjuvant, CT (List Biologic Laboratories, Campbell, CA), and two pro-inflammatory agents, dextran sodium sulfate (DSS, m.w. 36,000–50,000; ICN Biomedicals, Irvine, CA) and indomethacin (Sigma–Aldrich, St. Louis, MO), were used as stress-inducing agents to alter the intestinal environment of mice as described previously [17,23,24] (see Supplementary information).

2.4. Preparation of intestinal epithelial cells for FCM

The small intestinal epithelium was dissociated by a mechanical procedure as described previously [17]. The mononuclear cells were stained with NKM 16-2-4-FITC, UEA-1-PE and anti-CD45-APC and dead cells were stained with 7-aminoactinomycin D (BD Biosciences). Fluorescently labeled cells were analyzed and, if necessary, sort-purified using a FACSAria flow cytometer (BD Biosciences) (see Supplementary information).

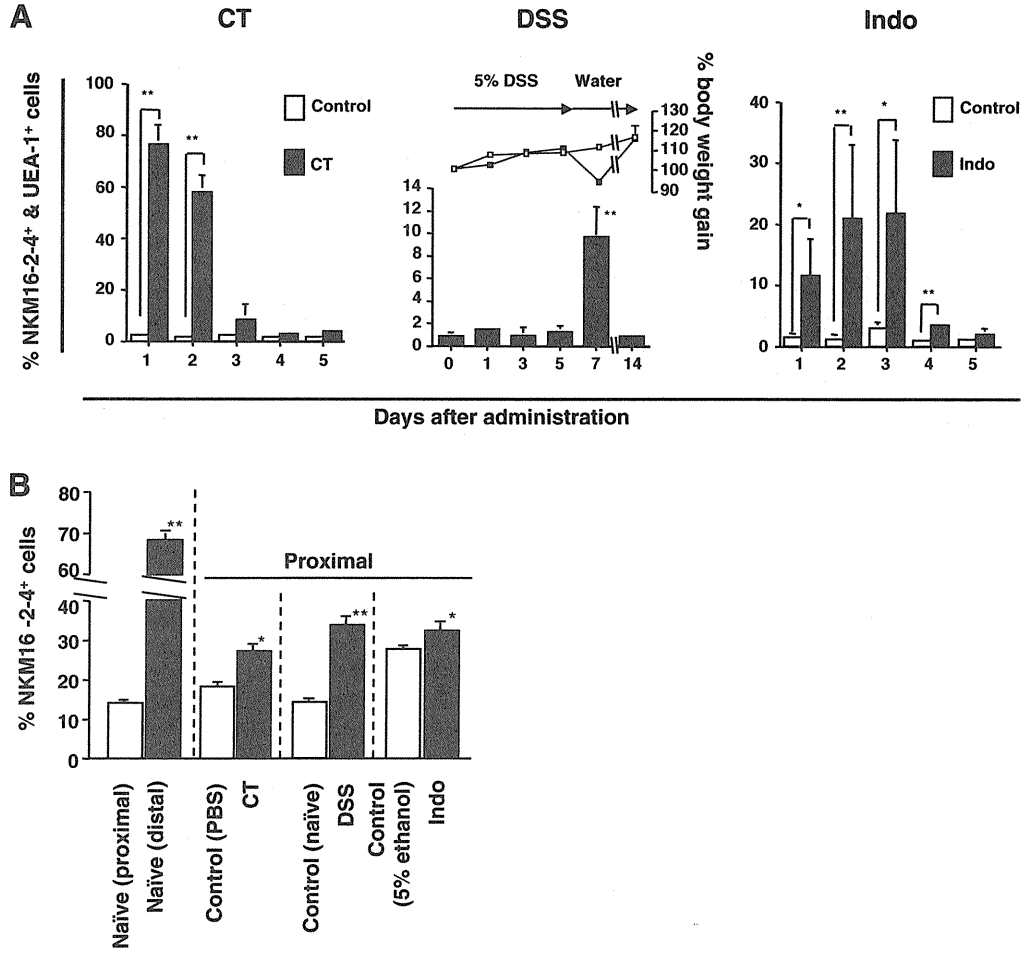

Fig. 1. The influence of IES on the induction of α(1,2)fucosylation in the small intestinal epithelia of BALB/c mice. (A) Daily analysis of the frequency of NKM 16-2-4$^+$/UEA-1$^+$ cells in the proximal villous epithelium of CT-, DSS- and indomethacin (Indo)-administered mice based on FCM. The ratio of NKM 16-2-4$^+$/UEA-1$^+$ cells was enumerated in cells, with 7-aminoactinomycin D$^+$ dead cells, CD45$^+$ leukocytes and small forward- and side-scattered lymphocytes gated out. The line graph in the middle panel shows the percentage body weight gain of control (open squares) and DSS-administered (filled squares) mice. Data are given as means ± SE (n = 3–7). Significant differences ($^*P < 0.05$, $^{**}P < 0.01$) were determined by t-test or Mann–Whitney's U test. (B) The proportions of NKM 16-2-4$^+$ cells in the PP domes based on histoplanimetrical analysis of CLSM images. Mice used were naïve, or were administered CT (day 1), DSS (day 7) or Indo (day 1). Data are given as means ± SE (n = 3, 19–76 domes). Significant differences ($^*P < 0.05$, $^{**}P < 0.01$) were determined by t-test.

2.5. Histological analysis

Fluorescently labeled whole-mount tissues were analyzed by CLSM as described previously [8,22]. Each area of NKM 16-2-4$^+$ cells and whole FAE in PPs was quantitated using Scion Image software (Scion Corporation, Frederick, MA) based on the data obtained by CLSM (see Supplementary information).

2.6. Quantitative real-time RT-PCR for Fut1 and Fut2 transcripts

The levels of the *Fut1* and *Fut2* transcripts were quantitated by real-time RT-PCR in the cDNA samples from the sorted cells with reference to the level of hypoxanthine guanine phosphoribosyl transferase (*Hprt*) transcripts (see Supplementary information).

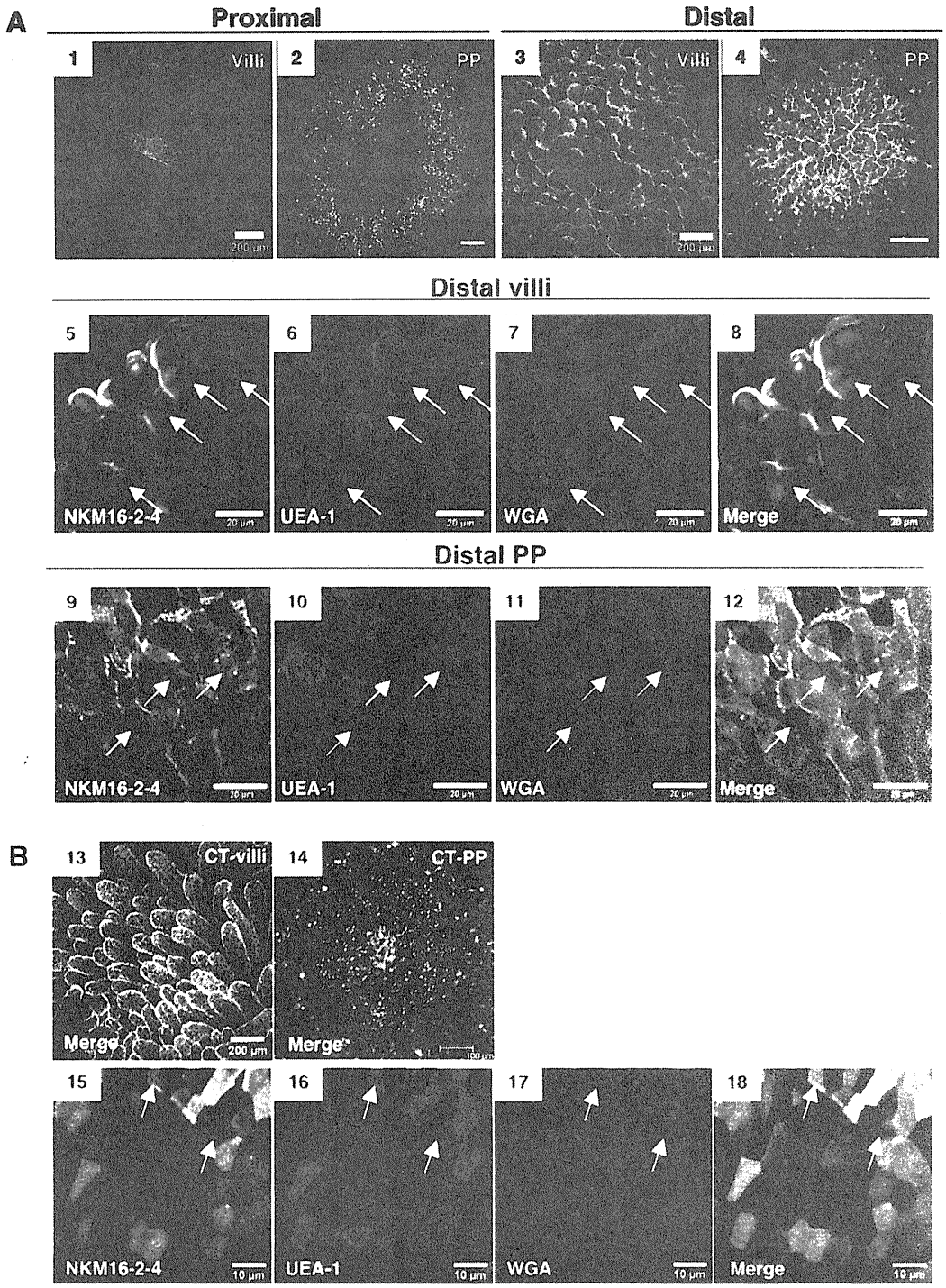

Fig. 2. CLSM analysis of whole-mount small intestinal epithelia of BALB/c mice. Confocal images stained with NKM 16-2-4-FITC, UEA-1-TRITC and WGA-AF633 are shown by green, red and blue, respectively. (A) Proximal villi (1) and PP (2), and distal villi (3, 5–8) and PP (4, 9–12) from naïve mice. (B) Proximal villi (13, 15–18) and PP (14), 1 day after oral CT administration. Arrows show villous M cells (NKM 16-2-4$^+$/UEA-1$^+$/WGA$^-$). Scale bars are 200 μm (1, 3, 13), 100 μm (2, 4, 14), 20 μm (5–12) or 10 μm (15–18). (For interpretation of the references to colour in this figure legend, the reader is referred to the web version of this article.)

2.7. Statistical analysis

The significance of the data was evaluated by the unpaired *t*-test, Mann–Whitney's U test, Tukey's or Scheffé's multiple comparison test based on the normality and variance of the data compared using Statcel2 software (OMS Publishing Inc., Saitama, Japan). $P < 0.05$ was considered statistically significant.

3. Results

3.1. Induction of α(1,2)fucosylation in the small intestinal epithelium by IES

To examine the influence of IES on M cell-associated α(1,2)fucosylation (NKM 16-2-4$^+$/UEA-1$^+$), we focused on the proximal epithelium, where NKM 16-2-4$^+$/UEA-1$^+$ cells were rarely found in naïve mice (Supplementary Fig. S1). When CT was orally administered to BALB/c mice, NKM 16-2-4$^+$/UEA-1$^+$ cells were dramatically increased in the proximal villous epithelium, with an average of 75.9% double-positive cells one day post-inoculation (Fig. 1A). The proportion of NKM 16-2-4$^+$/UEA-1$^+$ cells returned to the control level (approximately 2%) at 3 days post-inoculation. Similarly, a significant increase in NKM 16-2-4$^+$/UEA-1$^+$ cells was observed when pro-inflammatory agents, such as DSS or indomethacin, were administered (Fig. 1A).

A similar tendency was also seen in the FAE of PPs. We next performed histoplanimetrical analysis based on single NKM 16-2-4 signals obtained by CLSM. We previously demonstrated that NKM 16-2-4$^+$ cells included UEA-1$^+$ M cells but not goblet cells [22]. However, similar to UEA-1, because NKM 16-2-4 reacts to Paneth cells (Supplementary Fig. S2), NKM 16-2-4$^+$ cells were enumerated upward the crypts where Paneth cells locally exist. Therefore, goblet cells and Paneth cells were excluded in this analysis. When the proportions of NKM 16-2-4$^+$ cells were compared between the proximal and distal PP FAE of naïve BALB/c mice, a higher frequency of NKM 16-2-4$^+$ cells was observed in the distal (68.4%) than in the proximal (13.9%) PP FAE (Fig. 1B). Furthermore, a significant increase in NKM 16-2-4$^+$ cells was observed in the proximal PP FAE following CT-, DSS- or indomethacin-administration, averaging 27.2% (control: 18.1%), 33.8% (control: 13.9%) and 32.4% (control: 27.5%) positive cells, respectively (Fig. 1B). These results indicate that IES enhances α(1,2)fucosylation in both the PP FAE and the villous epithelium.

3.2. CLSM analysis of IES-induced NKM 16-2-4$^+$/UEA-1$^+$ cells

To assess qualitative cellular traits of IES-induced NKM 16-2-4$^+$/UEA-1$^+$ cells, we performed CLSM analysis using lectin WGA, which has an affinity for ECs and goblet cells but not M cells [6,8]. As indicated by FCM (Supplementary Fig. S1), a higher frequency of NKM 16-2-4$^+$/UEA-1$^+$ cells was observed in the distal (Fig. 2A; 3 and 4) than in the proximal villi and PPs (Fig. 2A; 1 and 2) in naïve BALB/c mice. In general, these NKM 16-2-4$^+$/UEA-1$^+$ cells were preferentially located at the tips of the villi (Fig. 2A; 1 and 3) and PP domes (Fig. 2A; 4) and a large proportion of them showed an affinity for WGA in both the villous epithelium (Fig. 2A; 7) and the PP FAE (Fig. 2A; 11), although a substantial number of villous M cells sharing the typical M cell hallmark (NKM 16-2-4$^+$/UEA-1$^+$/WGA$^-$) existed in the distal villi of naïve mice (Fig. 2A; 5–8: arrows).

The CLSM analysis further demonstrated that CT-induced NKM 16-2-4$^+$/UEA-1$^+$ cells also reacted with WGA (Fig. 2B). In contrast, villous M cells showing the M cell-phenotype (NKM 16-2-4$^+$/UEA-1$^+$/WGA$^-$) remained at a very low frequency irrespective of IES by CT (Fig. 2B; 15–18: arrows). A similar observation was made when DSS or indomethacin was administered (Supplementary Fig. S3). In the proximal PP FAE, whereas a substantial number of NKM 16-2-4$^+$/UEA-1$^+$ cells were negative for WGA and were radially distributed on the dome, indicating an M cell-phenotype (Fig. 2A; 2), triple-positive cells (NKM 16-2-4$^+$/UEA-1$^+$/WGA$^+$) were evident and were located on the tip of the dome after oral CT administration (Fig. 2B; 14). These results indicate that IES-induced NKM 16-2-4$^+$/UEA-1$^+$ cells share an affinity for WGA, a common trait of normal ECs [6], and hardly contain any villous M cells. We thus designated them fucosylated ECs (F-ECs), to distinguish them from typical M cells.

3.3. Different expression patterns of Fut1 and Fut2 transcripts in the small intestinal epithelium

To examine in more detail the mechanism of α(1,2)fucosylation between F-ECs and M cells, we performed quantitative real-time RT-PCR for *Fut1* and *Fut2* transcripts. Quantitative real-time RT-PCR demonstrated that high expression of *Fut1* transcripts was seen only in NKM 16-2-4$^+$/UEA-1$^+$ cells isolated from the naïve PP FAE where M cells predominantly exist (Fig. 3A). On the other hand, elevated expression of *Fut2* transcripts, but not *Fut1* transcripts, was detected in F-ECs located in the distal epithelia of naïve mice (Fig. 3A and B). Similarly, enhanced expression of *Fut2* transcripts, but not *Fut1* transcripts, was seen in CT-, DSS- and indomethacin-induced F-ECs of the proximal epithelia (Fig. 3A and B). These results indicate that α(1,2)fucosylation of F-ECs in the villous epithelium is induced by Fut2, and suggest that Fut1 is expressed in PP M cells irrespective of IES.

3.4. Distinct requirements for Fut1 or Fut2 for α(1,2)fucosylation of M cells or F-ECs, respectively

To clarify the distinct requirements for the Fut isoforms in F-ECs and M cells, Fut1-null and Fut2-null mice were employed for FCM

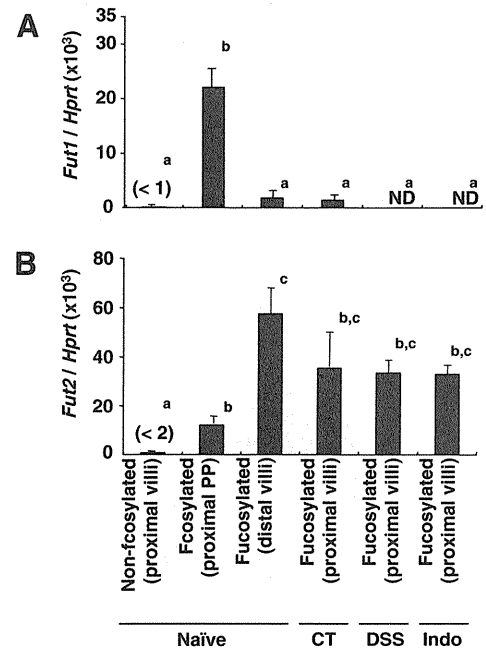

Fig. 3. Quantification of the expression levels of *Fut1* and *Fut2* transcripts relative to levels of *Hprt* transcripts. Fucosylated (NKM 16-2-4$^+$/UEA-1$^+$) and non-fucosylated (UEA-1$^-$) cells were purified from the proximal or distal small intestinal epithelia using a cell-sorter. Naïve, or CT- (Day 2), DSS- (Day 7) or indomethacin (Indo)- (Day 2) treated BALB/c mice were used. (A) *Fut1* transcripts. (B) *Fut2* transcripts. Data are given as means ± SE ($n = 3$–4). Different letters indicate significant differences ($P < 0.05$) determined by Tukey's multiple comparison test.

and CLSM analyses. Because these mice are on a C57BL/6J background [21], wild-type (WT) C57BL/6J mice were employed as a control group. Like BALB/c mice, WT C57BL/6J mice showed a higher frequency of F-ECs (NKM 16-2-4$^+$/UEA-1$^+$ cells) in the distal villous epithelium than in the proximal villous epithelium, and that the frequency of F-ECs in the latter increased after oral CT administration (Fig. 4A). This was also observed when Fut1-null mice were orally exposed to CT (Fig. 4A and C; 2 and 4). On the

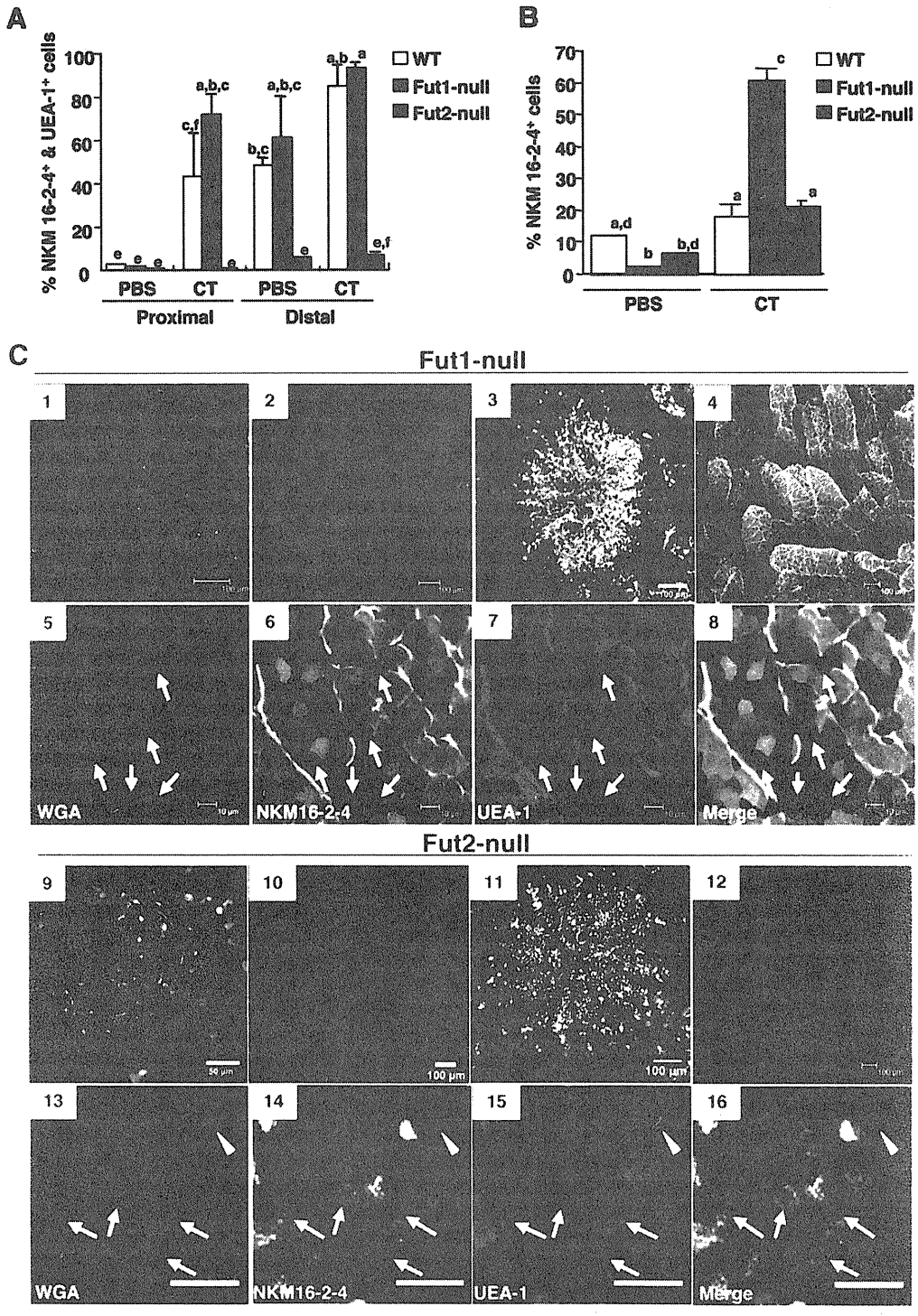

Fig. 4. Fut1- and Fut2-dependent α(1,2)fucosylation in PP M cells and F-ECs, respectively. (A) The proportions of NKM 16-2-4$^+$/UEA-1$^+$ cells in the proximal and distal villous epithelia of either day 1 PBS- or CT-administered (CT) WT C57BL/6J, Fut1-null and Fut2-null mice based on FCM as described in the Fig. 1 legend. Data are given as means ± SE (n = 3). Different letters indicate significant differences ($P < 0.05$) determined by Tukey's multiple comparison test. (B) The proportions of NKM 16-2-4$^+$ cells in the proximal PP domes based on histoplanimetrical analysis of CLSM images. WT, Fut1-null and Fut2-null mice were used after oral administration of either PBS or CT (day 1). Data are given as means ± SE (n = 3, 12–25 domes). Different letters indicate significant differences ($P < 0.05$) determined by Scheffé's multiple comparison test. (C) CLSM analysis for the whole-mount small intestinal epithelia of either naïve or day 1 CT-treated Fut1-null (naïve; 1, 2, CT; 3–8) and Fut2-null mice (naïve; 9, 10, CT; 11–16). Confocal images stained with NKM 16-2-4-FITC, UEA-1-TRITC and WGA-AF633 are shown by green, red and blue, respectively. Arrows and arrowheads indicate WGA$^-$ PP M cells and Fut1-dependent WGA$^+$ cells, respectively. Scale bars are 100 μm (1–4, 10–12), 50 μm (9), 20 μm (13–16) or 10 μm (5–8). (For interpretation of the references to colour in this figure legend, the reader is referred to the web version of this article.)

other hand, Fut2-null mice possessed few NKM 16-2-4$^+$/UEA-1$^+$ cells in the villous epithelia and the number of these cells was not increased upon oral CT administration (Fig. 4A and C; 10 and 12). PBS-administered Fut2-null mice showed 0.1% and 4.9% of NKM 16-2-4$^+$/UEA-1$^+$ cells in the proximal and distal villous epithelia, respectively, and CT-administered Fut2-null mice showed 0.3% and 5.3% in the proximal and distal villous epithelia, respectively (Fig. 4A).

In contrast to the villous epithelia, the PP FAE contained both types of fucosylated cells, dependent on either Fut1 or Fut2. In PBS-administered conditions, 2.0% and 6.3% of NKM 16-2-4$^+$ cells were observed in the proximal PP FAE of Fut1-null and Fut2-null mice, respectively (Fig. 4B). Oral CT administration did not notably induce α(1,2)fucosylation in the PP FAE of WT mice; CT-administered and PBS-administered WT mice contained 17.8% and 12.0% of NKM 16-2-4$^+$ cells, respectively, and there was no statistical difference between the two groups (Fig. 4B). However, both Fut1-null and Fut2-null mice showed significant induction of NKM 16-2-4$^+$ cells in the proximal PP FAE, with the proportion of positive cells being 60.5% and 21.0%, respectively (Fig. 4B). CLSM analysis further revealed that the fucosylation of M cells was dependent on Fut1, because WGA$^-$ M cells did not induce α(1,2)fucosylation and thus did not react with either NKM 16-2-4 or UEA-1 in Fut1-null mice (Fig. 4C; 1, 3 and 5–8: arrows) whereas they did react with these markers in Fut2-null mice (Fig. 4C; 9, 11 and 13–16: arrows) irrespective of oral CT administration. In addition, the fucosylation of F-ECs in the PP FAE was dependent on Fut2 because triple-positive cells (NKM 16-2-4$^+$/UEA-1$^+$/WGA$^+$ cells) were preferentially observed in the CT-administered Fut1-null mice (Fig. 4C; 3 and 5–8). Although a small number of Fut1-dependent WGA$^+$ cells were observed in the PP FAE of CT-administered Fut2-null mice (Fig. 4C; 13–16: arrowheads), they were distributed radially, accompanying abundant WGA$^-$ M cells on the PP dome (Fig. 4C; 11), and were distinguishable from the Fut2-dependent F-ECs that were distributed all over the dome (Fig. 4C; 3).

Taken together, these results indicate that α(1,2)fucosylation of PP M cells is dependent on Fut1 irrespective of IES, and that Fut2 is involved in α(1,2)fucosylation of F-ECs residing in both the PP FAE and villous epithelium in response to IES.

4. Discussion

In this study, we showed that intestinal environmental and biological stress induced F-ECs, which were recognized by NKM 16-2-4 and UEA-1, in both the PP FAE and the villous epithelium. However, such IES-induced F-ECs possessed a strong affinity for WGA (Fig. 2). In addition, F-ECs showed the same morphological characteristics as ECs such as columnar architecture, well-developed tall and dense microvilli (Supplementary Fig. S4), and did not possess *Salmonella* uptake-ability (Supplementary Fig. S5). Furthermore, F-ECs did not express glycoprotein 2 (Supplementary Fig. S6 and Table S1), recently identified as an M cell-specific molecule [17,25]. Therefore, F-ECs should be distinguished from typical M cells, and IES-induced α(1,2)fucosylation reflects only a phenotypic change of surface glycosylation pattern that is irrelevant to M-cell differentiation.

The requirements for different fucosylation-inducing enzymes clearly demonstrated a distinction between F-ECs and PP M cells: Fut1 is essential for the fucosylation associated with PP M cells while Fut2 is specifically involved in the fucosylation of IES-induced F-ECs in both the PP FAE and villous epithelium (Fig. 4). Although it has been reported that the expression of *Fut1* transcripts is rare and is not induced or altered in the small intestine by the transfer from germ-free to conventional conditions [11,18–20], these results are probably due to the low frequency of PP M cells throughout the small intestine. In contrast, it has been known that *Fut2* transcripts are induced in the small intestine, particularly in the ileum, of mice in response to colonization by commensal bacteria or treatment with a protein synthesis inhibitor [11,19]. Our present data, in which IES resulted in the induction of Fut2-dependent F-ECs, is consistent with and support these previous findings.

Fut1 and Fut2 provide insights into the involvement of IES in the development of not only F-ECs but also M cells. The PP dome epithelium consists of two cell lineages: one is derived from the dome-associated crypts and differentiates into either M cells or ECs, and the other is derived from villus-associated crypts and differentiates into ECs [26]. In addition, some studies have revealed a dynamic and plastic morphology of M cells; for example, the distinctive microfold and membranous structures occur transiently during the cell differentiation process, and M cell-lineage cells in their early and terminal development stages show the same morphological structure as ECs [27,28]. In this study, we showed a possibility that Fut1-dependent fucosylated cells are increased by IES (Fig. 4). These cells consisted of abundant PP M cells and a few WGA$^+$ EC-like cells, both of which were distributed radially on the dome. To this end, we suggest a possibility that Fut1-dependent cells are M cell-lineage cells derived from the dome-associated crypts that participate in the increase of M cells in response to IES, as described elsewhere [12–15]. In contrast to PP M cells, the fucosylation of villous M cells, like F-ECs, is regulated by Fut2 because α(1,2)fucosylation in the villi was not observed in Fut2-null but Fut1-null mice regardless of oral CT administration (Fig. 4 and Supplementary Table S1). However, IES alone would not influence the frequency of villous M cells because oral CT administration did not induce *Salmonella* uptake in the villi (Supplementary Fig. S5). It has recently been shown that receptor activator of nuclear factor-kappa B ligand (RANKL) is capable of the full development of both PP and villous M cells but RANKL-expressing inducer cells preferentially exist in the subepithelial dome of PPs [29]. Taken together, transient IES alone might be insufficient for the recruitment and/or induction of RANKL-expressing cells in the villi, and/or other factors might be required for the full development of villous M cells.

Although specific functions of F-ECs remain to be elucidated, our present study offers the possibility that Fut1-null and Fut2-null mice would provide a direct opportunity to examine *in vivo* the immuno-biological role of F-ECs and M cells, including their specific fucosylated glycans, towards a better understanding of the gut mucosal immune system.

Acknowledgments

We thank Dr. Osamu Igarashi for technical support and Dr. Rebecca Devon for editing the manuscript. This work was supported in part by Grants from the Ministry of Education, Science, Sports and Culture of Japan (H.K. and K.T.), and the Ministry of Health, Labour and Welfare of Japan (H.K.).

Appendix A. Supplementary data

Supplementary data associated with this article can be found, in the online version, at doi:10.1016/j.bbrc.2010.12.067.

References

[1] M.R. Neutra, A. Frey, J.P. Kraehenbuhl, Epithelial M cells: gateways for mucosal infection and immunization, Cell 86 (1996) 345–348.
[2] H. Hamada, T. Hiroi, Y. Nishiyama, et al., Identification of multiple isolated lymphoid follicles on the antimesenteric wall of the mouse small intestine, J. Immunol. 168 (2002) 57–64.
[3] R.L. Owen, A.L. Jones, Epithelial cell specialization within human Peyer's patches: an ultrastructural study of intestinal lymphoid follicles, Gastroenterology 66 (1974) 189–203.

[4] M.R. Neutra, N.J. Mantis, A. Frey, et al., The composition and function of M cell apical membranes: implications for microbial pathogenesis, Semin. Immunol. 11 (1999) 171–181.
[5] J.P. Kraehenbuhl, M.R. Neutra, Epithelial M cells: differentiation and function, Annu. Rev. Cell Dev. Biol. 16 (2000) 301–332.
[6] M.A. Clark, M.A. Jepson, N.L. Simmons, et al., Differential expression of lectin-binding sites defines mouse intestinal M-cells, J. Histochem. Cytochem. 41 (1993) 1679–1687.
[7] M.A. Clark, M.A. Jepson, N.L. Simmons, et al., Selective binding and transcytosis of Ulex europaeus 1 lectin by mouse Peyer's patch M-cells in vivo, Cell Tissue Res. 282 (1995) 455–461.
[8] M.H. Jang, M.N. Kweon, K. Iwatani, et al., Intestinal villous M cells: an antigen entry site in the mucosal epithelium, Proc. Natl. Acad. Sci. USA 101 (2004) 6110–6115.
[9] Y. Umesaki, M. Ohara, Factors regulating the expression of the neutral glycolipids in the mouse small intestinal mucosa, Biochim. Biophys. Acta 1001 (1989) 163–168.
[10] L. Bry, P.G. Falk, T. Midtvedt, et al., A model of host-microbial interactions in an open mammalian ecosystem, Science 273 (1996) 1380–1383.
[11] B. Lin, Y. Hayashi, M. Saito, et al., GDP-fucose: beta-galactoside alpha1,2-fucosyltransferase, MFUT-II, and not MFUT-I or -III is induced in a restricted region of the digestive tract of germ-free mice by host-microbe interactions and cycloheximide, Biochim. Biophys. Acta 1487 (2000) 275–285.
[12] M.W. Smith, P.S. James, D.R. Tivey, M cell numbers increase after transfer of SPF mice to a normal animal house environment, Am. J. Pathol. 128 (1987) 385–389.
[13] T.C. Savidge, M.W. Smith, P.S. James, et al., Salmonella-induced M-cell formation in germ-free mouse Peyer's patch tissue, Am. J. Pathol. 139 (1991) 177–184.
[14] C. Borghesi, M.J. Taussig, C. Nicoletti, Rapid appearance of M cells after microbial challenge is restricted at the periphery of the follicle-associated epithelium of Peyer's patch, Lab. Invest. 79 (1999) 1393–1401.
[15] T. Kucharzik, A. Lugering, N. Lugering, et al., Characterization of M cell development during indomethacin-induced ileitis in rats, Aliment. Pharmacol. Ther. 14 (2000) 247–256.
[16] J. Mach, T. Hshieh, D. Hsieh, et al., Development of intestinal M cells, Immunol. Rev. 206 (2005) 177–189.
[17] K. Terahara, M. Yoshida, O. Igarashi, et al., Comprehensive gene expression profiling of Peyer's patch M cells, villous M-like cells and intestinal epithelial cells, J. Immunol. 180 (2008) 7840–7846.
[18] S.E. Domino, N. Hiraiwa, J.B. Lowe, Molecular cloning, chromosomal assignment and tissue-specific expression of a murine alpha(1,2)-fucosyltransferase expressed in thymic and epididymal epithelial cells., Biochem. J. 327 (Pt 1) (1997) 105–115.
[19] M. Iwamori, S.E. Domino, Tissue-specific loss of fucosylated glycolipids in mice with targeted deletion of alpha(1, 2)fucosyltransferase genes, Biochem. J. 380 (2004) 75–81.
[20] B. Lin, M. Saito, Y. Sakakibara, et al., Characterization of three members of murine alpha1,2-fucosyltransferases: change in the expression of the Se gene in the intestine of mice after administration of microbes, Arch. Biochem. Biophys. 388 (2001) 207–215.
[21] S.E. Domino, L. Zhang, P.J. Gillespie, et al., Deficiency of reproductive tract alpha(1,2)fucosylated glycans and normal fertility in mice with targeted deletions of the FUT1 or FUT2 alpha(1,2)fucosyltransferase locus, Mol. Cell. Biol. 21 (2001) 8336–8345.
[22] T. Nochi, Y. Yuki, A. Matsumura, et al., A novel M cell-specific carbohydrate-targeted mucosal vaccine effectively induces antigen-specific immune responses, J. Exp. Med. 204 (2007) 2789–2796.
[23] I. Okayasu, S. Hatakeyama, M. Yamada, et al., A novel method in the induction of reliable experimental acute and chronic ulcerative colitis in mice, Gastroenterology 98 (1990) 694–702.
[24] T. Kunikata, H. Araki, M. Takeeda, et al., Prostaglandin E prevents indomethacin-induced gastric and intestinal damage through different EP receptor subtypes, J. Physiol. Paris 95 (2001) 157–163.
[25] K. Hase, K. Kawano, T. Nochi, et al., Uptake through glycoprotein 2 of FimH(+) bacteria by M cells initiates mucosal immune response, Nature 462 (2009) 226–230.
[26] A. Gebert, S. Fassbender, K. Werner, et al., The development of M cells in Peyer's patches is restricted to specialized dome-associated crypts, Am. J. Pathol. 154 (1999) 1573–1582.
[27] S. Onishi, T. Yokoyama, K. Chin, et al., Ultrastructural study on the differentiation and the fate of M cells in follicle-associated epithelium of rat Peyer's patch, J. Vet. Med. Sci. 69 (2007) 501–508.
[28] F. Sierro, E. Pringault, P.S. Assman, et al., Transient expression of M-cell phenotype by enterocyte-like cells of the follicle-associated epithelium of mouse Peyer's patches, Gastroenterology 119 (2000) 734–743.
[29] K.A. Knoop, N. Kumar, B.R. Butler, et al., RANKL is necessary and sufficient to initiate development of antigen-sampling M cells in the intestinal epithelium, J. Immunol. 183 (2009) 5738–5747.

frontiers in MICROBIOLOGY

ORIGINAL RESEARCH ARTICLE
published: 10 January 2012
doi: 10.3389/fmicb.2011.00280

Fluorescent reporter signals, EGFP, and DsRed, encoded in HIV-1 facilitate the detection of productively infected cells and cell-associated viral replication levels

Kazutaka Terahara[1], Takuya Yamamoto[2], Yu-ya Mitsuki[1,3], Kentaro Shibusawa[1,3], Masayuki Ishige[1,4], Fuminori Mizukoshi[5], Kazuo Kobayashi[1] and Yasuko Tsunetsugu-Yokota[1]*

[1] Department of Immunology, National Institute of Infectious Diseases, Tokyo, Japan
[2] The Immunology Laboratory, Vaccine Research Center, National Institute of Allergy and Infectious Diseases, National Institutes of Health, Bethesda, MD, USA
[3] Research Resident, Japan Foundation for AIDS Prevention, Tokyo, Japan
[4] Division of Hematopoiesis, Center for AIDS Research, Kumamoto University, Kumamoto, Japan
[5] Department of Microbiology, The Tochigi Prefectural Institute of Public Health and Environmental Science, Tochigi, Japan

Edited by:
Hirofumi Akari, Kyoto University, Japan

Reviewed by:
Mikako Fujita, Kumamoto University, Japan
Jun-Ichi Sakuragi, Osaka University, Japan

***Correspondence:**
Yasuko Tsunetsugu-Yokota, Department of Immunology, National Institute of Infectious Diseases, 1-23-1 Toyama, Shinjuku-ku, Tokyo 162-8640, Japan.
e-mail: yyokota@nih.go.jp

Flow cytometric analysis is a reliable and convenient method for investigating molecules at the single cell level. Previously, recombinant human immunodeficiency virus type 1 (HIV-1) strains were constructed that express a fluorescent reporter, either enhanced green fluorescent protein, or DsRed, which allow the monitoring of HIV-1-infected cells by flow cytometry. The present study further investigated the potential of these recombinant viruses in terms of whether the HIV-1 fluorescent reporters would be helpful in evaluating viral replication based on fluorescence intensity. When primary CD4$^+$ T cells were infected with recombinant viruses, the fluorescent reporter intensity measured by flow cytometry was associated with the level of CD4 downmodulation and Gag p24 expression in infected cells. Interestingly, some HIV-1-infected cells, in which CD4 was only moderately downmodulated, were reporter-positive but Gag p24-negative. Furthermore, when the activation status of primary CD4$^+$ T cells was modulated by T cell receptor-mediated stimulation, we confirmed the preferential viral production upon strong stimulation and showed that the intensity of the fluorescent reporter within a proportion of HIV-1-infected cells was correlated with the viral replication level. These findings indicate that a fluorescent reporter encoded within HIV-1 is useful for the sensitive detection of productively infected cells at different stages of infection and for evaluating cell-associated viral replication at the single cell level.

Keywords: HIV-1, flow cytometry, EGFP, DsRed, Gag, productive infection

INTRODUCTION

Human immunodeficiency virus type 1 (HIV-1) interacts with its primary receptor, CD4, and a co-receptor, usually CCR5 or CXCR4, to infect T cells, macrophages, and dendritic cells (Mcclure et al., 1987; Berger et al., 1999; Tsunetsugu-Yokota, 2008). Single cell analysis of HIV-1-infected cells is an essential approach to investigate the differential dynamics of HIV-1 infection and the cellular consequences for each of the HIV-1-targeted cell populations. To monitor HIV-1 infection, a recombinant HIV-1 encoding a reporter luciferase (Luc) gene, or indicator cells transduced with enzymatic reporters such as Luc, β-galactosidase, alkaline phosphatase, and chloramphenicol acetyl transferase, incorporated downstream of the HIV-1 long terminal repeats (LTR) have been widely used (Kar-Roy et al., 2000). However, these reporters require additional substrates or co-factors, and lysis or fixation of cells is required to show reporter activity, which makes the experimental process more complex. In addition, it is difficult to distinguish infected cells from uninfected cells using these reporter assays.

An alternative molecule, green fluorescent protein (GFP) and/or its derivatives, is a powerful reporter that does not require any substrates and co-factors to generate a reporter signal (Chalfie, 1995; Cubitt et al., 1995; Heim et al., 1995). Page et al. (1997) first used a GFP derivative, called enhanced green fluorescent protein (EGFP), as a fluorescent reporter molecule for HIV-1 and showed that infected cells were detectable and, more importantly, distinguishable from uninfected cells using flow cytometry. Furthermore, a red fluorescent protein, DsRed, has been used as an HIV-1 fluorescent reporter (Weber et al., 2006). The main benefit of such recombinant HIV-1 molecules is that the targeted cells do not require any modulation (e.g., transfection) of exogenous reporter genes and, therefore, they allow the characterization of intact HIV-1-infected cells. In most cases of previous recombinant HIV-1 strains, the *nef* gene was replaced with a reporter gene. Therefore, we previously constructed *nef*-intact, replication-competent, recombinant HIV-1 strains encoding either EGFP or DsRed, and showed that CXCR4-tropic X4 and CCR5-tropic R5 viruses replicate differently in CD4$^+$ T cells simultaneously infected with X4 HIV-1 encoding EGFP and R5 HIV-1 encoding

DsRed (Yamamoto et al., 2009). Such recombinant HIV-1 strains encoding a fluorescent reporter gene will be even more valuable because of recent advances in multicolor flow cytometry, which permit more detailed characterization of HIV-1-infected cells.

Flow cytometry is a reliable and convenient method for analysis at the single cell level. Because the transcriptional activity of HIV-1 can be quantitatively monitored in indicator cells according to the fluorescence intensity of an EGFP reporter driven by the HIV-1 LTR (Dorsky et al., 1996; Gervaix et al., 1997; Kar-Roy et al., 2000), we investigated whether the HIV-1-expressing fluorescent reporters EGFP and DsRed would allow the quantitative evaluation of viral replication using a flow cytometer. The results show that a fluorescent reporter signal generated by recombinant HIV-1 strains enables the detection of infected cells at various stages of the viral life cycle.

MATERIALS AND METHODS

CELL PREPARATION

Human peripheral blood samples were collected from healthy donors after written informed consent. Sample collection was approved by the Institutional Ethical Committee of the National Institute of Infectious Diseases (NIID; Tokyo, Japan). Peripheral blood mononuclear cells (PBMCs) were separated on a Ficoll–Hypaque density gradient (Lymphosepal; IBL, Gunma, Japan) and $CD4^+$ T cells were negatively selected from the PBMCs using an EasySep Human $CD4^+$ T cell Enrichment Kit (StemCell Technologies, Vancouver, BC, Canada).

CEM cells stably expressing human CCR5 (CEM–CCR5) were established by transducing CEM cells with the human *ccr5* gene using a conventional mouse retrovirus system. CEM–CCR5 cells were maintained in complete RPMI medium (10% heat-inactivated fetal bovine serum, 100 μg/ml penicillin, 100 μg/ml streptomycin, and 2 mM L-glutamine) supplemented with 1 μg/ml puromycin at 37°C.

PREPARATION OF HIV-1 VIRUS STOCKS

We previously constructed pNL432-based proviral clones encoding EGFP (pNL-E) or DsRed (pNL-D) for X4-tropic HIV-$1_{NL\text{-}E}$ or HIV-$1_{NL\text{-}D}$, respectively, and pNLAD8-based proviral clones encoding EGFP (pNLAD8-E) or DsRed (pNLAD8-D) for R5-tropic HIV-$1_{NLAD8\text{-}E}$ or HIV-$1_{NLAD8\text{-}D}$, respectively (Yamamoto et al., 2009; **Figure 1**). To prepare the HIV-1 viral stocks, the human embryonic kidney cell line 293T was transfected with pNL-E, pNL-D, pNLAD8-E, or pNLAD8-D using the calcium phosphate precipitation method and then incubated for 48 h. Culture supernatants were filtered and frozen at −80°C. The amount of virus in each culture supernatant was measured using an in-house HIV-1 Gag p24 enzyme-linked immunosorbent assay (ELISA; Tsunetsugu-Yokota et al., 1995).

STIMULATION OF T CELL RECEPTORS

T cell receptors (TCR) were stimulated as described previously (Yamamoto et al., 2009) with some modifications. In brief, primary $CD4^+$ T cells were suspended in complete RPMI medium supplemented with 5% human plasma and stimulated with 5 μg/ml of immobilized anti-human CD3 monoclonal antibody (mAb; eBioscience, San Diego, CA) and 1 μg/ml of soluble anti-human CD28 mAb (eBioscience) in U-bottom, 96-well plates at 37°C for 4 (weak stimulation) or 24 h (strong stimulation).

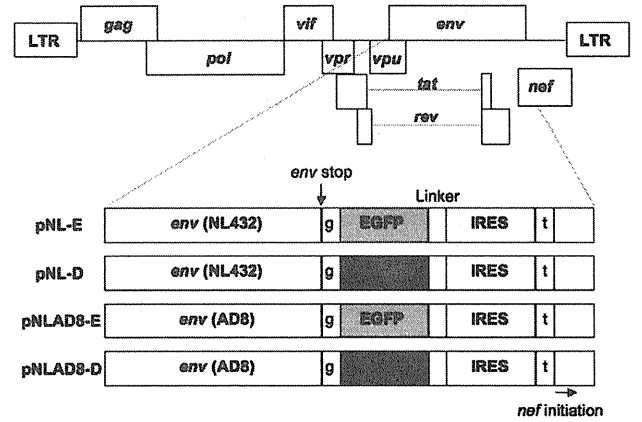

FIGURE 1 | Structure of the proviral DNA. The pNL432-based proviral clones encoded EGFP (pNL-E) or DsRed (pNL-D) for X4-tropic HIV-$1_{NL\text{-}E}$ or HIV-$1_{NL\text{-}D}$, respectively, and the pNLAD8-based proviral clones encoded EGFP (pNLAD8-E) or DsRed (pNLAD8-D) for R5-tropic HIV-$1_{NLAD8\text{-}E}$ or HIV-$1_{NLAD8\text{-}D}$, respectively. EGFP or DsRed was not expressed as a fusion protein with Env due to the insertion of a single base after the Env stop codon. Nef was also independently expressed under the control of IRES. t (Thymine) and g (guanine) are additional DNA sequences.

HIV-1 INFECTION AND CELL CULTURE

Primary $CD4^+$ T cells (either unstimulated or pre-TCR-stimulated) or CEM–CCR5 cells were infected with 200 ng of p24-measured amounts of HIV-$1_{NL\text{-}E}$, HIV-$1_{NL\text{-}D}$, HIV-$1_{NLAD8\text{-}E}$, or HIV-$1_{NLAD8\text{-}D}$ per 1×10^6 cells by spinoculation at $1200 \times g$ for 2 h at 25 (conventional conditions) or 4°C (for CEM–CCR5 cells), as described previously (O'doherty et al., 2000; Dai et al., 2009). After spinoculation, cells were washed three times with PBS. Primary $CD4^+$ T cells were then suspended in complete RPMI medium supplemented with 5% human plasma. The cell suspensions derived from unstimulated or pre-TCR-stimulated $CD4^+$ T cells were settled onto U-bottom, 96-well plates with or without TCR-stimulation, respectively, at 37°C for 24 h. After the 24 h culture, cells were washed three times with PBS, suspended in complete RPMI medium supplemented with 5% human plasma and 50 U/ml recombinant interleukin-2, and cultured in U-bottom, 96-well plates at 37°C for up to 4 days.

FLOW CYTOMETRY

Cells were stained with fluorescence-conjugated mAbs as described previously (Yamamoto et al., 2009). The following mAbs were used for flow cytometry in various combinations: Pacific Blue-conjugated anti-human CD3 mAb (BioLegend, San Diego, CA, USA), phycoerythrin Cy7-conjugated anti-human CD4 mAb (BioLegend), and Alexa Fluor 700-conjugated anti-human CD8a mAb (BioLegend); and Nu24 mAb specific for HIV-1 Gag p24 (kindly provided by Dr. T. Sata, NIID, Tokyo, Japan) and conjugated to Alexa Fluor 647 using an Alexa Fluor 647 Protein Labeling Kit (Molecular Probes, Eugene, OR, USA). Dead cells were stained with propidium iodide or a LIVE/DEAD Fixable Dead Cell Stain

Kit (L34957; Invitrogen, Carlsbad, CA, USA). Intracellular staining (ICS) by Nu24 mAb was performed using a FIX and PERM Fixation and Permeabilization Kit (Invitrogen). Data collection was performed using a FACSCanto II (BD Bioscience, San Diego, CA, USA) and the data were analyzed using FACSDiva software (BD Bioscience) and FlowJo software (Tree Star, San Carlos, CA, USA).

QUANTIFICATION OF REPLICATED HIV-1 IN CELL CULTURE SUPERNATANTS

Human immunodeficiency virus type 1 replication was quantified in cell culture supernatants by ELISA and real-time RT-PCR. Gag p24 was measured using a RETRO-TEK HIV-1 p24 Antigen ELISA (ZeptoMetrix Corporation, Buffalo, NY, USA). For real-time RT-PCR, viral RNA was extracted using a QIAamp Viral RNA Mini Kit (Qiagen, Valencia, CA, USA) and subjected to real-time RT-PCR using a SuperScript III Platinum One-Step Quantitative RT-PCR System (Invitrogen), a set of HIV-1 *gag*-targeted primers, and a TaqMan probe as previously described (Saito et al., 2010). PCR was performed in an Mx3000P (Stratagene, La Jolla, CA, USA).

RESULTS

CD4 DOWNMODULATION IS ASSOCIATED WITH HIV-1 FLUORESCENT REPORTER INTENSITY

The cell surface CD4 molecule is downmodulated in HIV-1-infected cells in response to the HIV-1 components Env, Nef, and Vpu (Malim and Emerman, 2008). Therefore, to investigate the correlation between the level of CD4 downmodulation and the HIV-1 fluorescent reporter intensity, primary $CD4^+$ T cells infected with HIV-$1_{NL\text{-}E}$, HIV-$1_{NL\text{-}D}$, HIV-$1_{NLAD8\text{-}E}$, or HIV-$1_{NLAD8\text{-}D}$ followed by TCR-stimulation for 1 day and cultivation for a further 4 days were analyzed by flow cytometry. As shown in **Figure 2** (left panels), HIV-1-infected cells expressing a fluorescent reporter signal, EGFP, or DsRed, were detected, although the numbers varied between individual donors ($n = 3$–4): about 10–30% for X4-tropic HIV-$1_{NL\text{-}E}$-infected and HIV-$1_{NL\text{-}D}$-infected cells and 1–10% for R5-tropic HIV-$1_{NLAD8\text{-}E}$-infected and HIV-$1_{NLAD8\text{-}D}$-infected cells. However, the number of HIV-1^+ cells was comparable between HIV-$1_{NL\text{-}E}$ and HIV-$1_{NL\text{-}D}$ (X4-tropic), and between HIV-$1_{NLAD8\text{-}E}$ and HIV-$1_{NLAD8\text{-}D}$ (R5-tropic) within each donor, showing that the fluorescent reporter genes encoded within the HIV-1 proviral genome did not affect HIV-1 infectivity as described previously (Yamamoto et al., 2009). When we categorized $CD3^+CD8^-$ T cells into three fractions (HIV-1-negative, -dull, and -high) based on the fluorescence intensity of EGFP and DsRed, we found that CD4 was strongly downmodulated in the HIV-1 high fraction in all the HIV-1 strains (**Figure 2**, right panels). Interestingly, CD4 was also downmodulated in the HIV-1 dull fraction, but the level was modest compared with that in the HIV-1 high fraction (**Figure 2**, right panels). These results indicate that the level of CD4 downmodulation is associated with HIV-1 fluorescent reporter intensity.

FIXATION/PERMEABILIZATION WEAKENS THE HIV-1 FLUORESCENT REPORTER SIGNAL

To investigate the correlation between HIV-1 fluorescent reporter intensity and viral replication levels, we attempted to perform ICS for Gag p24 in HIV-1-infected cells prepared as described above. When we observed X4-tropic HIV-$1_{NL\text{-}E}$-infected and HIV-$1_{NL\text{-}D}$-infected cells from three donors by flow cytometry, we noticed that fixation/permeabilization, an essential step for ICS, weakened the fluorescent reporter signal for both EGFP and DsRed. **Figure 3** shows the flow cytometry profiles obtained for EGFP and DsRed at identical photomultiplier tube (PMT) voltages between intact (untreated) cells and fixed/permeabilized cells to visualize the differences in fluorescent reporter intensity. $DsRed^+$ cells were not properly separated from $DsRed^-$ cells within the population treated by fixation/permeabilization; the frequency of $DsRed^+$ cells was, therefore, markedly decreased. No adjustment of the flow cytometer settings, including PMT voltage and compensation, improved the blunted fluorescent reporter signal generated after fixation/permeabilization. Nevertheless, the number of $EGFP^+$ cells within the intact cell and fixed/permeabilized cell populations was comparable. Similar results were obtained for R5-tropic HIV-$1_{NLAD8\text{-}E}$ and HIV-$1_{NLAD8\text{-}D}$ (data not shown). Taken together, these results indicate that it is preferable to use an EGFP reporter when the fixation/permeabilization of cells is required.

HIV-1 FLUORESCENT REPORTER SIGNALS RELIABLY DETECT PRODUCTIVELY INFECTED CELLS SHOWING DIFFERENT VIRAL REPLICATION LEVELS

Following the results shown in **Figure 3**, we next assessed viral replication levels in the HIV-$1_{NL\text{-}E}$ infection group (5 days culture) from six donors using Gag p24 ICS (**Figure 4**). A representative flow cytometric analysis showed that not all $EGFP^+$ cells were Gag^+ and *vice versa*. When CD4 expression levels were compared in each of the four cell fractions based on the expression patterns of EGFP and Gag p24 ($EGFP^+Gag^+$, $EGFP^+Gag^-$, $EGFP^-Gag^+$, and $EGFP^-Gag^-$), the strongest downmodulation of CD4 was observed in $EGFP^+Gag^+$ cells (red fraction). CD4 downmodulation was moderate in $EGFP^+Gag^-$ cells (green fraction). However, CD4 was not downmodulated at all in $EGFP^-Gag^+$ cells (blue fraction) and the expression level of CD4 was the same as that in $EGFP^-Gag^-$ cells (black fraction). We further divided the $EGFP^+Gag^+$ cells (red fraction) into Gag^{hi} (brown fraction) and Gag^{lo} cells (pink fraction) and compared the expression levels of EGFP and CD4 with those of Gag p24. Gag^{hi} cells (brown fraction) showed the strongest expression of EGFP and the strongest downmodulation of CD4. Gag^{lo} cells (pink fraction) showed an intermediate level of EGFP expression [between that of Gag^{hi} cells (brown fraction) and that of $EGFP^+Gag^-$ cells (green fraction)] and CD4 expression [between that of Gag^{hi} cells (brown fraction) and $EGFP^-Gag^-$ cells (black fraction)]. These results indicate that the expression level of EGFP correlates with that of Gag p24 in HIV-1-infected cells in which CD4 is downmodulated.

HIV-1-BOUND OR -INTERNALIZED CELLS ARE ALSO DETECTED BY Gag p24 ICS

Because CD4 downmodulation was not observed in $EGFP^-Gag^+$ cells (**Figure 4**; blue fraction), it is possible that these cells may still be bound by or have internalized HIV-1 but have not produced virions. Therefore, we next investigated the kinetics of $EGFP^-Gag^+$ cells during 5 days post-infection. Primary $CD4^+$

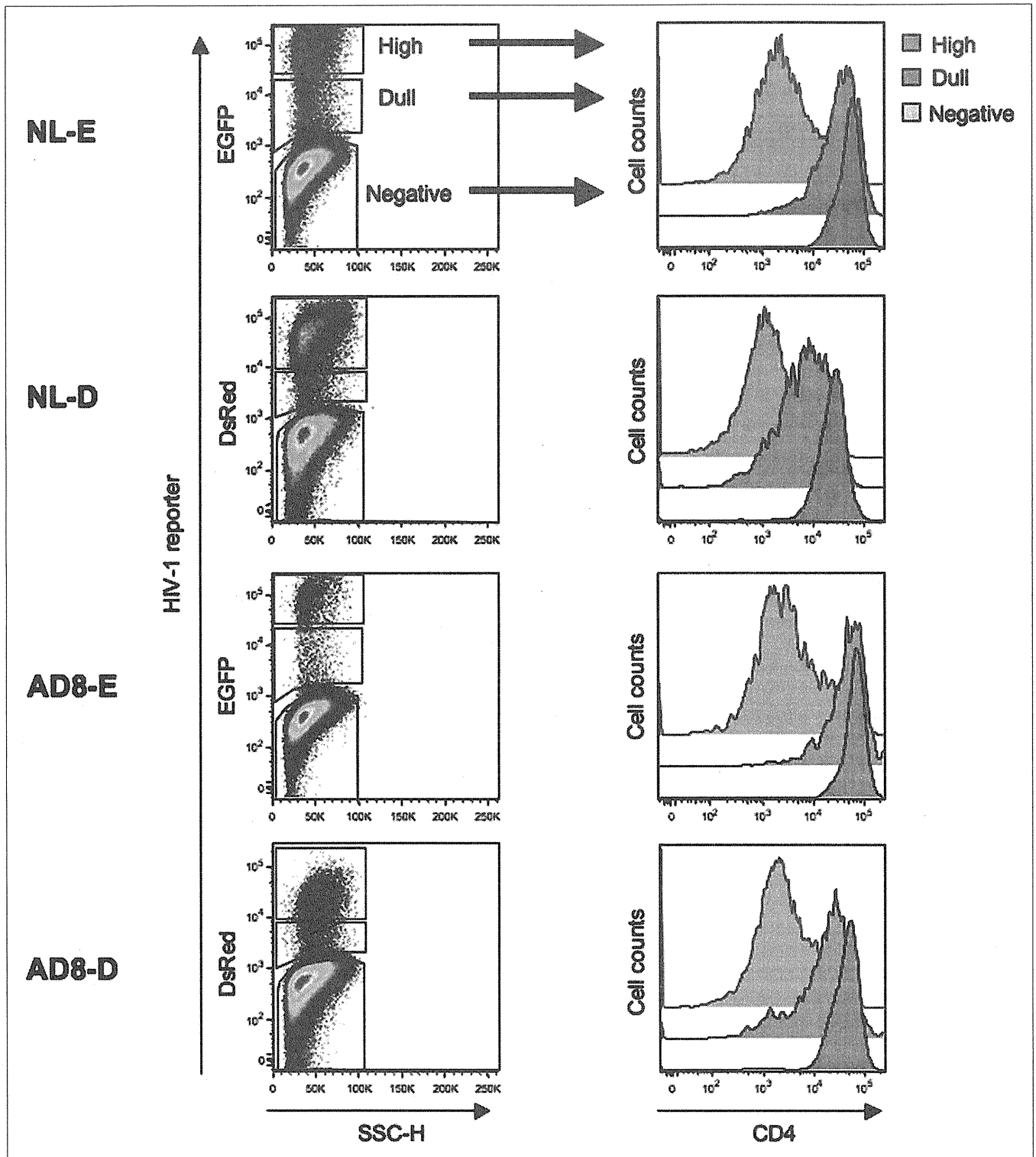

FIGURE 2 | Flow cytometry analysis of HIV-1-infected cells. Unstimulated CD4+ T cells were infected with HIV-1_{NL-E}, HIV-1_{NL-D}, HIV-$1_{NLAD8-E}$, or HIV-$1_{NLAD8-D}$ and cultured for 5 days (including the initial 1 day culture with TCR-stimulation). (Left panels) representative pseudo-color plot profiles for the $Dead^-/CD3^+/CD8^-$-gated cell fractions from three donors. Cells were classified as high (red), dull (blue), and negative (black) based on the HIV-1 reporter intensity. (Right panels) histograms of CD4 expression by the high (red), dull (blue), and negative (black) fractions defined.

T cells from three donors were infected with HIV-1_{NL-E} followed by TCR-stimulation for 1 day and cultivation for a further 4 days. **Figure 5A** shows a representative flow cytometric analysis. At 1 day post-infection, 17.6% of Gag $p24^+$ cells were observed,

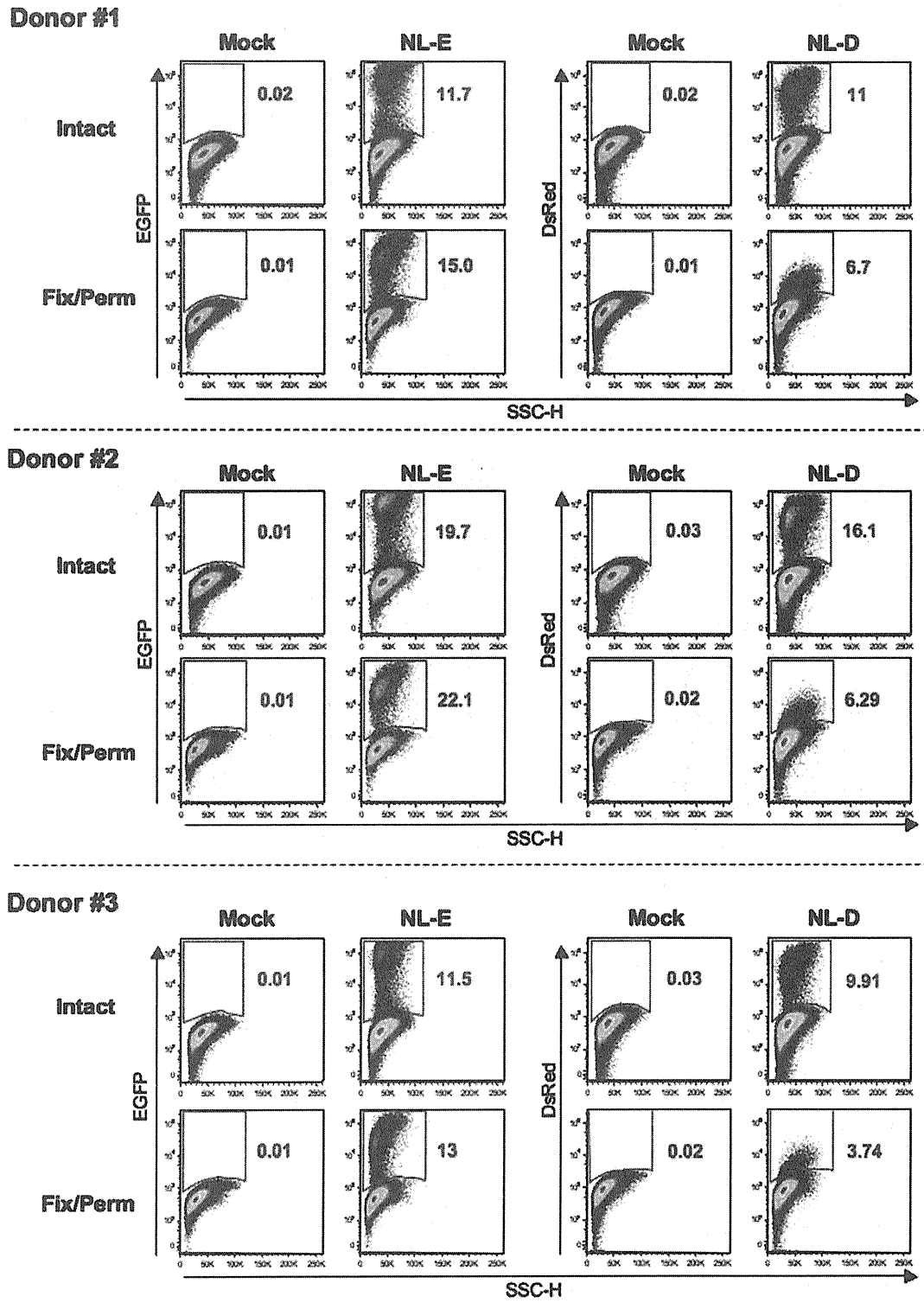

FIGURE 3 | Influence of fixation/permeabilization treatment on HIV-1 fluorescent reporter signals. Pseudo-color plot profiles for the Dead$^-$/CD3$^+$/CD8$^-$-gated cell fractions from the mock, HIV-1$_{NL-E}$ infection (NL-E), and HIV-1$_{NL-D}$ infection (NL-D) groups from all three donors tested. Analyzed cells were prepared as outlined in the legend to **Figure 2** and then either fixed/permeabilized (fix/perm) or not (intact).

despite the fact that no EGFP$^+$ cells were detected. At 2 days post-infection, the proportion of EGFP$^-$Gag$^+$ cells was decreased and EGFP$^+$ cells including Gag p24$^+$ and Gag p24$^-$ cells became to be observed, suggesting that initially infecting HIV-1 was

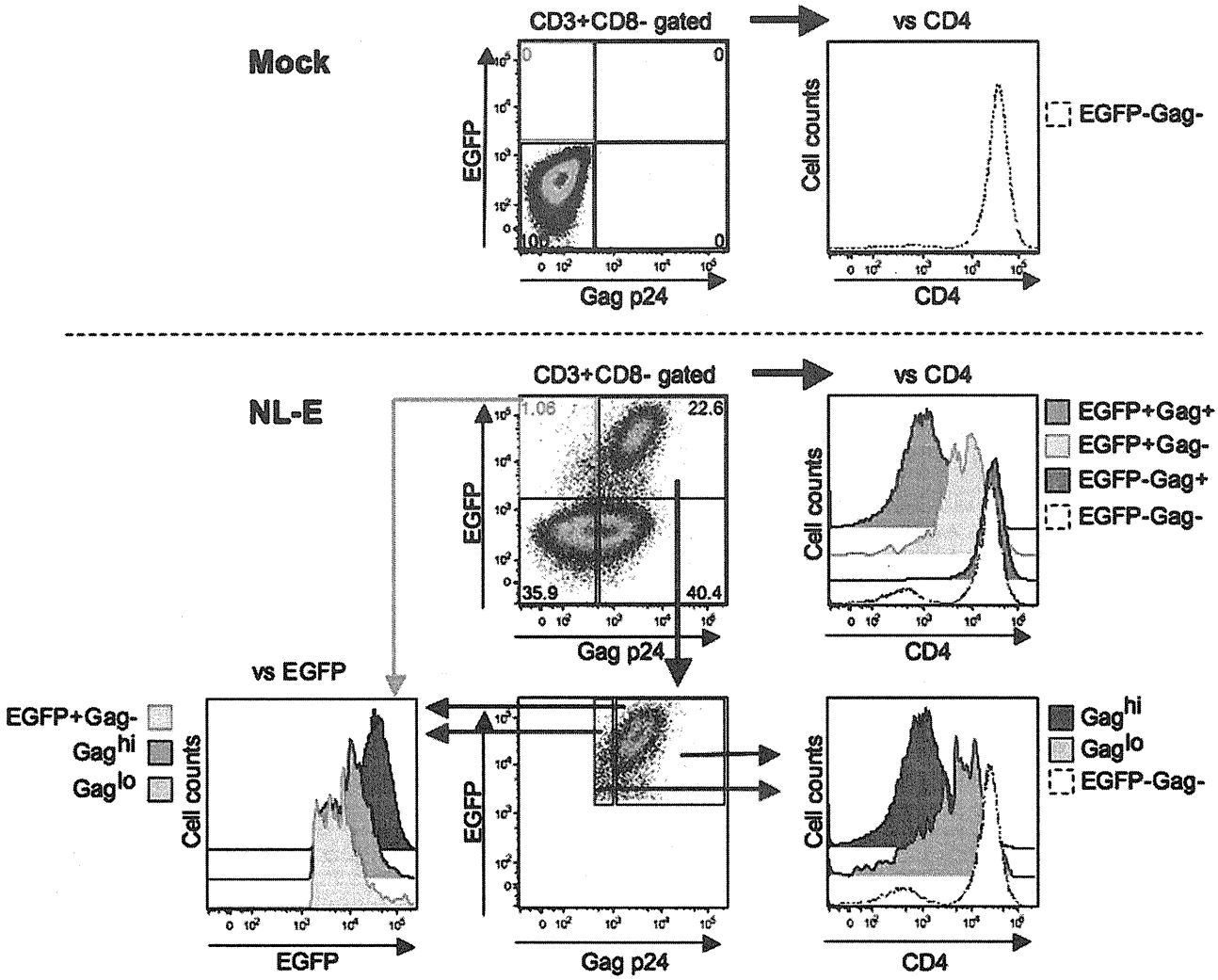

FIGURE 4 | Correlation between HIV-1 fluorescent reporter signal and Gag p24 expression. Representative flow cytometric analyses of the mock and HIV-1_{NL-E} infection groups from six donors. These infection groups were prepared as outlined in the legend to **Figure 2**. The $EGFP^+Gag^+$ (red), $EGFP^+Gag^-$ (green), $EGFP^-Gag^+$ (blue), $EGFP^-Gag^-$ (black), Gag^{hi} (brown), and Gag^{lo} (pink) cell fractions were categorized based on the expression patterns of EGFP and Gag p24. The expression levels of CD4 and EGFP in each cell fraction were compared according to their histogram profiles.

degraded and/or replaced with replication-competent proviruses. After 3 days post-infection, $EGFP^+$ cells were clearly visible and the proportion of $EGFP^-Gag^+$ cells turned to be increased, suggesting that progeny virus infection occurred. Because the CD4 expression levels were identical between $EGFP^-Gag^+$ cells and $EGFP^-Gag^-$ cells throughout the culture period, Gag p24 ICS must have detected cells that had bound or internalized HIV-1.

CEM–CCR5 cells, which are almost as susceptible to X4 and R5 HIV-1 fusion (data not shown), were used to confirm that Gag p24 ICS did indeed detect HIV-1-bound cells. Also, because it has been suggested that spinoculation at 25°C may induce HIV-1 fusion to the targeted cells (Dai et al., 2009), we tested Gag p24 ICS using CEM–CCR5 cells immediately after spinoculation with X4-tropic HIV-1_{NL-E} or R5-tropic HIV-1_{AD8-E} at 4°C. When cells were not fixed/permeabilized, no Gag $p24^+$ cells were detected by flow cytometry (**Figure 5B**, upper panels); however, when cells were fixed/permeabilized, a substantial proportion of Gag^+ cells was detectable in both the HIV-1_{NL-E} and HIV-1_{AD8-E} infection groups (**Figure 5B**, lower panels). Taken together, these results indicate that cells that have bound or internalized HIV-1 can be detected using flow cytometry for Gag p24 ICS.

THE INTENSITY OF THE HIV-1 FLUORESCENT REPORTER SIGNAL DEPENDS ON TCR-MEDIATED ACTIVATION LEVELS

T cell receptors-mediated activation of HIV-1-infected $CD4^+$ T cells increased productive viral replication, although the signaling pathway responsible may be different for X4 and R5 HIV-1 (Popik and Pitha, 2000). We investigated whether the intensity of the HIV-1 fluorescent reporter signal was affected by TCR-mediated

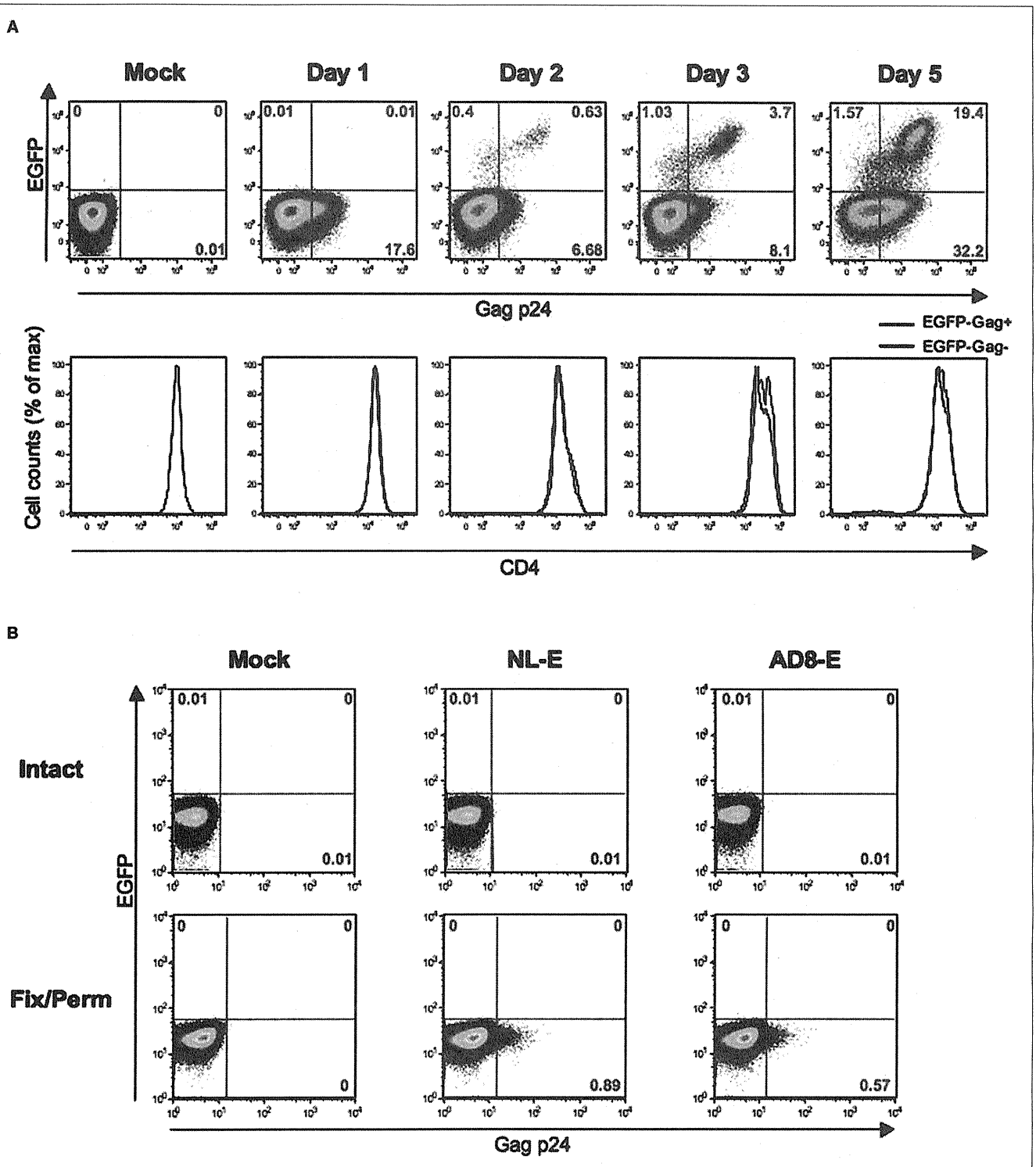

FIGURE 5 | Evaluation of Gag p24 ICS for HIV-1-internalized and -bound cells. (A) Representative flow cytometric analyses of the HIV-1_{NL-E} infection (NL-E) and mock (Mock) groups from three donors in which unstimulated primary $CD4^+$ T cells were infected with HIV-1_{NL-E} or not, respectively, and cultured for 5 days (including the initial 1 day culture with TCR-stimulation). The expression patterns of EGFP and Gag p24 are indicated in the pseudo-color plot profiles for the $Dead^-/CD3^+/CD8^-$-gated cell fractions (upper panels). The expression level of CD4 in $EGFP^-Gag^+$ and $EGFP^-Gag^-$ cells is indicated in the histograms by the blue and black lines, respectively (lower panels). **(B)** Representative flow cytometric analyses of Gag p24 staining. CEM–CCR5 cells were infected with HIV-1_{NL-E} (NL-E), HIV-1_{AD8-E} (AD8-E), or not (Mock). Immediately after spinoculation at 4°C, the cells were washed and fixed/permeabilized (fix/perm) or not (intact) prior to Gag p24 staining.